

國立交通大學
光電工程研究所
碩士論文

超快時間解析反射技術研究氮砷化銦鎵單層量子井

The Ultrafast Time-Resolved Photoreflectance
Measurement of $\text{InGaAs}_x\text{N}_{1-x}$ Single Quantum Wells



研究生：林盈秀
指導教授：謝文峰教授

中華民國九十四年六月

超快時間解析反射技術研究氮砷化銦鎵 單層量子井

The Ultrafast Time-Resolved Photoreflectance Measurement of
InGaAs_xN_{1-x} Single Quantum Wells

研究生：林盈秀

Student: Ying-Hsiu Lin

指導教授：謝文峰 教授

Advisor: Dr. Wen-Feng Hsieh



A Thesis

Submitted to Institute of Electro-Optical Engineering

College of Electrical Engineering and

Computer Science

National Chiao Tung University

in Partial Fulfillment of the Requirements

for the Degree of

Master

in

Electro-optical Engineering

June 2005

Hsin-chu, Taiwan, Republic of China

中華民國九十四年六月


超快時間解析反射技術研究氮砷化銦鎵 單層量子井

研究生：林 盈 秀

指導教授：謝 文 峰 教授

國立交通大學光電工程研究所

摘要



在本論文中，我們比較由金屬有機化學氣相沈積法(MOCVD)成長的砷化銦鎵和氮砷化銦鎵單層量子井的超快載子動力學。從螢光光譜的量測，我們可以發現氮砷化銦鎵的能隙因為氮的加入比砷化銦鎵的能隙小很多，可以發出波長為 $1.3\mu\text{m}$ 的光。我們利用飛秒時析反射量測研究載子的鬆弛過程。比較這兩個樣品的量測結果，我們發現在氮砷化銦鎵的載子生命期比在砷化銦鎵的短。這可能是因為載子鬆弛過程中，載子被加入氮所造成的缺陷捕捉所導致。

The Ultrafast Time Resolved Photoreflectance Measurement of $\text{InGaAs}_x\text{N}_{1-x}$ Single Quantum Wells

Student: Ying-Hsiu Lin

Advisor: Dr. Wen-Feng Hsieh

Institute of Electro-Optical Engineering

National Chiao Tung University

Abstract

The comparative analysis of the ultrafast carrier dynamics of metal-organic chemical vapor deposition (MOCVD) grown $\text{In}_{0.4}\text{Ga}_{0.6}\text{As}$ and $\text{In}_{0.4}\text{Ga}_{0.6}\text{As}_{0.995}\text{N}_{0.005}$ single quantum wells (SQW) is reported. From photoluminescence (PL) measurement we conclude that the incorporation of a low content N in InGaAsN reduces the band-gap energy significantly and allows emission wavelengths shift to 1.3 μm . Carrier dynamics were investigated by femtosecond time-resolved photoreflectance measurement at 800 nm with various pump intensities. Comparison with these two samples indicates that the carrier relaxation in the $\text{In}_{0.4}\text{Ga}_{0.6}\text{As}_{0.995}\text{N}_{0.005}$ SQW is dominated by defect traps associated with the N incorporation.

致謝

時光飛逝，兩年的碩士生活，隨著這本論文寫出來，已接近尾聲。兩年來不管是專業知識方面還是待人處事的態度都有進步，當然要感謝最多的就是我的指導教授謝文峰教授。如果沒有老師不厭其煩的教導，我想我不會得到這麼多。另外一方面老師帶領學生的風氣也很棒，讓實驗室不會死氣沈沈，而是在努力研究之餘還能充滿歡笑！

隨著兩年的朝夕相處，和實驗室的大家，從不熟悉到熟悉，從有形象到不顧形象，現在，要離開還真有點捨不得呢！家弘學長、政哥、奎哥、小戴學長、智章學長、鄭信民學長、黃董、維仁、松哥、碩一唯一的學弟：展榕、實驗室另一朵花：潘晴如學姐，謝謝你們在實驗上、課業上和生活上的幫助。另外，同甘苦共患難的碩二的同伴：國峰、俊毅、家斌、小豪、文勛，謝謝你們在實驗和課業方面的互相切磋討論。我會一直一直記得國峰幫我殺了很多小強，和小毅非常直接的意見的！真的是謝謝大家，讓我的碩士生涯如此豐富。

本論文得以完成，要感謝的人還很多：子安學長、亞銜學長、伯宗學弟在實驗技巧上的說明、贊伯出借儀器、親愛的爸媽的贊助讓我生活不虞匱乏，我只能說，沒有你們，就沒有我啊！再多的言語也沒有辦法表達清楚我心中滿溢的感謝！

最後感謝國科會計畫 NSC-93-2112-M-009-035 對於此研究的支持以及贊助。

盈秀（阿笑） 風城交大筆 94.7.5

Content

Abstrate(in Chinese).....	I
Abstrate (in English).....	II
Acknowledgements.....	III
Content.....	IV
List of figures.....	VI
List of Tables.....	VII
Chapter 1 Introduction.....	1
1.1 Introduction.....	1
1.1.1 InGaAsN/GaAs Heterostructures.....	1
1.1.2 Semiconductor Carrier Dynamics.....	1
1.1.3 Femtosecond Time-Resolved Spectroscopy.....	2
1.2 Aim of This Thesis.....	3
Chapter 2 Femtosecond Time-Resolved Systems	7
2.1 Pump-Probe Transmission/Reflection Spectroscopy.....	7
2.2 Time-Resolved Photoluminescence (PL) Spectroscopy.....	8
2.3 Time-Resolved Terahertz-Probe Spectroscopy.....	9
Chapter 3 Ultrafast Spectroscopy of Semiconductor	12
3.1 Basic Concepts.....	12
3.1.1 Scattering Processes in Semiconductors.....	12
3.1.2 Carrier Relaxation in Photoexcited Semiconductors.....	13
3.2 Ultrafast Phenomena of Semiconductors.....	15
3.2.1 Bulk GaAs.....	15
3.2.2 InGaAsN/GaAs.....	16
3.3 Carrier-Induced Change in Refractive Index.....	18

3.3.1	Band Filling	18
3.3.2	Bandgap Renormalization.....	19
3.3.3	Free-Carrier Absorption	21
Chapter 4	Experiments.....	23
4.1	InGaAsN Single Quantum Well Structures.....	23
4.1.1	Mode-Locked Ti:sapphire laser	24
4.1.2	Autocorrelator	24
4.1.3	Experimental Setup of Femtosecond Time-Resolved Measurement	24
4.1.4	Zero Delay Point.....	25
Chapter 5	Results and Discussion	31
5.1	Ultrafast Time Resolved Photoreflectance of Bulk GaAs	32
5.2	Ultrafast Time Resolved Photoreflectance of InGaAs _{1-x} N _x SQW	34
Chapter 6	Conclusion and Perspectives.....	40
Appendix I	Fitting results of bulk GaAs	41
Appendix II	Fitting results of SQW (I).....	42
Appendix III	Fitting results of SQW (II).....	43
References	44

List of Figures

Fig. 1-1 The electron-hole pair creation following excitation of a semiconductor with laser radiation of energy $\hbar\omega_0$	4
Fig. 1-2 The block diagram illustrating the follow of energy in a photoexcited semiconductor.	4
Fig. 1-3 Illustrating different time-scale measurements require different time-resolution tools.	5
Fig. 1-4 Schematic diagram of the shortest pulses reported versus year	5
Fig. 2-1 Schematic for a generic setup for a two-beam nonlinear experiment	10
Fig. 3-1 Four temporally-overlapping relaxation regime in photoexcited semiconductors.	22
Fig. 4-1 Cross-sectional schematic conduction band diagram of the $\text{In}_{0.4}\text{Ga}_{0.6}\text{As}_{1-x}\text{N}_x$ SQW	27
Fig. 4-2 HRTEM image of $\text{In}_{0.4}\text{Ga}_{0.6}\text{As}_{0.995}\text{N}_{0.005}/\text{GaAs}$ SQW	27
Fig. 4-3 Result of photoluminescence (PL) spectra measurement.	28
Fig. 4-4 The optical beam path within Coherent Mira-900.	28
Fig. 4-5 Sketch diagram of the intensity autocorrelator	29
Fig. 4-6 The autocorrelation trace	29
Fig. 4-7 Femtosecond time-resolved photoreflectance measurement system.	30
Fig. 5-1 Pump-intensity dependent time-resolved photoreflectance of bulk GaAs.	36
Fig. 5-2 The measured ΔR peak amplitude versus pump power in bulk GaAs.	36
Fig. 5-3 The normalized ΔR traces of bulk GaAs with various pump power.	37
Fig. 5-4 The carrier lifetime versus pump power in bulk GaAs.	37
Fig. 5-5 The pump-intensity dependent time-resolved photoreflectance of $\text{In}_{0.4}\text{Ga}_{0.6}\text{As}$ SQW and $\text{In}_{0.4}\text{Ga}_{0.6}\text{As}_{0.995}\text{N}_{0.005}$ SQW at 800 nm.	38
Fig. 5-6 The measured ΔR peak amplitude versus pump power of $\text{In}_{0.4}\text{Ga}_{0.6}\text{As}$ SQW and $\text{In}_{0.4}\text{Ga}_{0.6}\text{As}_{0.995}\text{N}_{0.005}$ SQW	39

List of Tables

Table 1-1 Fundamental processes in semiconductors.....	6
Table 1-2 List of the application of time-resolved spectroscopy.....	6
Table 5-1 List of carrier lifetimes of $\text{In}_{0.4}\text{Ga}_{0.6}\text{As}$ SQW and $\text{In}_{0.4}\text{Ga}_{0.6}\text{As}_{0.995}\text{N}_{0.005}$ SQW with various pump power.....	39



Chapter 1 Introduction

1.1 Introduction

1.1.1 InGaAsN/GaAs Heterostructures

InGaAsN/GaAs heterostructures are attracting much interest because of their highly nonlinear effects upon nitrogen incorporation [1] and their potential for long wavelength optoelectronic device application [2][3][4]. The large band offsets in InGaAsN quaternary alloy lead to the improvement of temperature performance, better than conventional InP-based materials [5][6]. The challenge to demonstrate devices of superior performance is at present dependent on improving the optical and structural quality of the dilute nitride quantum wells. Structural imperfections are most likely responsible for the significant increase of the monomolecular recombination rate in InGaAsN compared with InGaAs [7]. In addition, the carrier dynamics is strongly affected by N incorporation, as shown in the few studies reported in the literature [8][9][10][11]. Consequently, understanding the influence of nitrogen in InGaAsN is very valuable.

1.1.2 Semiconductor Carrier Dynamics

On the past few decades, there have been tremendous advancements in the field of ultrafast carrier dynamics in semiconductors [12]. The driving force behind this movement other than the basic fundamental interest is the direct application of semiconductor devices and the endless need for the faster response and the faster processing of information. To improve and to develop high-speed microelectronics devices, there must be a basic understanding of the various dynamical processes in the

semiconductors. Therefore, the excitation of semiconductors out of their equilibrium and the subsequent relaxation processes with various rates become a key area of semiconductor research. Linear absorption takes place when the photon energy is larger than the fundamental energy gap of the semiconductor as shown in Fig. 1-1. Following optical excitation, electrons and holes undergo spatial and temporal evolution with characteristic times which depend on the various relaxation processes. Table 1-1 lists the fundamental processes and Fig. 1-2 shows the energy relaxation follows in a photoexcited semiconductor. With the development of lasers that can generate pulses as short as a few femtoseconds the excitation and the subsequent probing of semiconductors on an ultrafast time scale have become routine.

1.1.3 Femtosecond Time-Resolved Spectroscopy

Fig. 1-3 illustrating that different time-scale measurements require different time-resolution tools. For measuring the velocity of a running tortoise, it is enough to use minute-resolution clock. For measuring the velocity of a running human, a second-resolution stopwatch is required. However, only the femtosecond-resolution pump-probe technique with ultrashort laser could achieve the measurement of electron lifetime between various energy bands. In the past decade, the technology of generating and detecting short optical pulses has advanced substantially. As shown schematically in Fig. 1-4, the width of optical pulses has fallen by more than 3 orders of magnitude since 1966. Systems such as the colliding pulse mode-lock (CPM) laser developed by Fork and Shank [13] have made possible ultrafast semiconductor measurements with femtosecond resolution. The applications of time-resolved spectroscopy in several fields are listed in Table 1-2.

1.2 Aim of This Thesis

In this thesis, we report the ultrafast time-resolved photoreflectance of $\text{In}_{0.4}\text{Ga}_{0.6}\text{As}_{1-x}\text{N}_x/\text{GaAs}$ single quantum wells. We compare the ultrafast time-resolved photoreflectance measurements in samples differing in the N incorporation ($x = 0\%$ and $x = 0.5\%$). We also measure the ultrafast time-resolved photoreflectance of bulk GaAs. All the results of our measurements are shown and discussed in chapter 5.

In chapter 2 and chapter 3, we briefly describe the ultrafast time-resolved pump-probe system and ultrafast spectroscopy of semiconductor. In chapter 4, the investigated sample structure and the experimental setup of ultrafast time-resolved measurement are discussed in details. Finally, the conclusion and perspectives are both given in chapter 6.



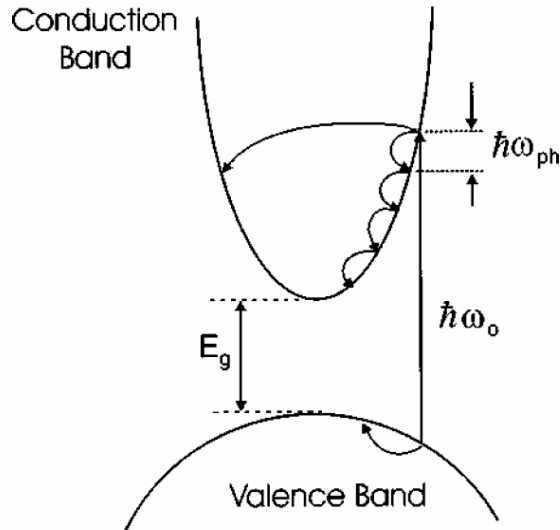


Fig. 1-1 The electron-hole pair creation following excitation of a semiconductor with laser radiation of energy $\hbar\omega_0$. Energy relaxation follows via optical phonon emission ($\hbar\omega_{ph}$).

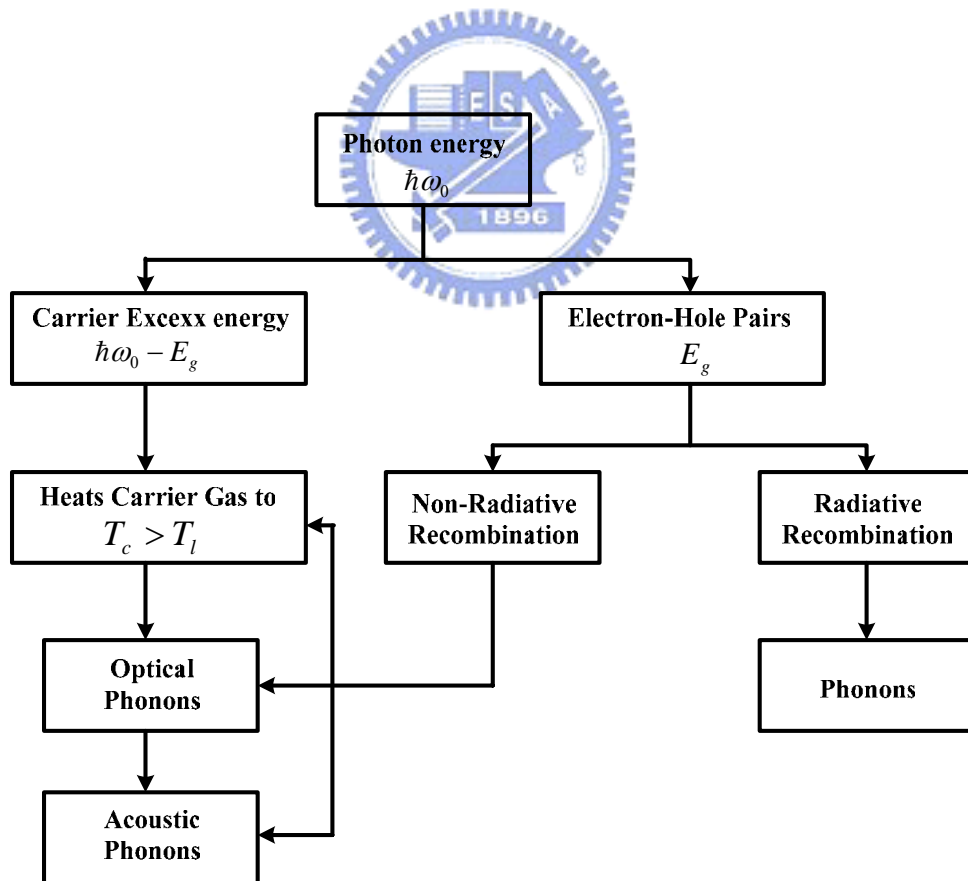


Fig. 1-2 The block diagram illustrating the follow of energy in a photoexcited semiconductor.

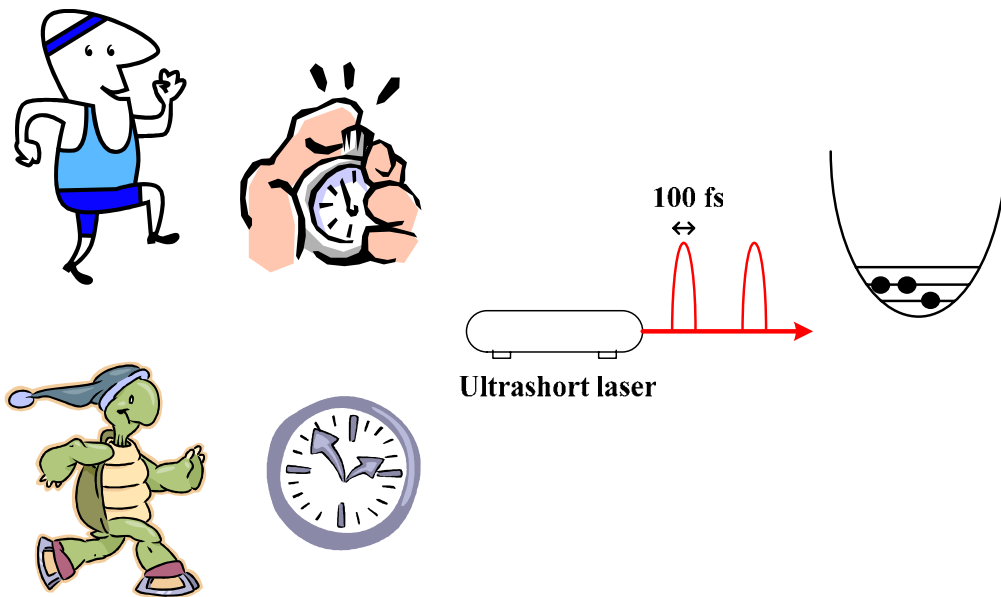


Fig. 1-3 Illustrating different time-scale measurements require different time-resolution tools.

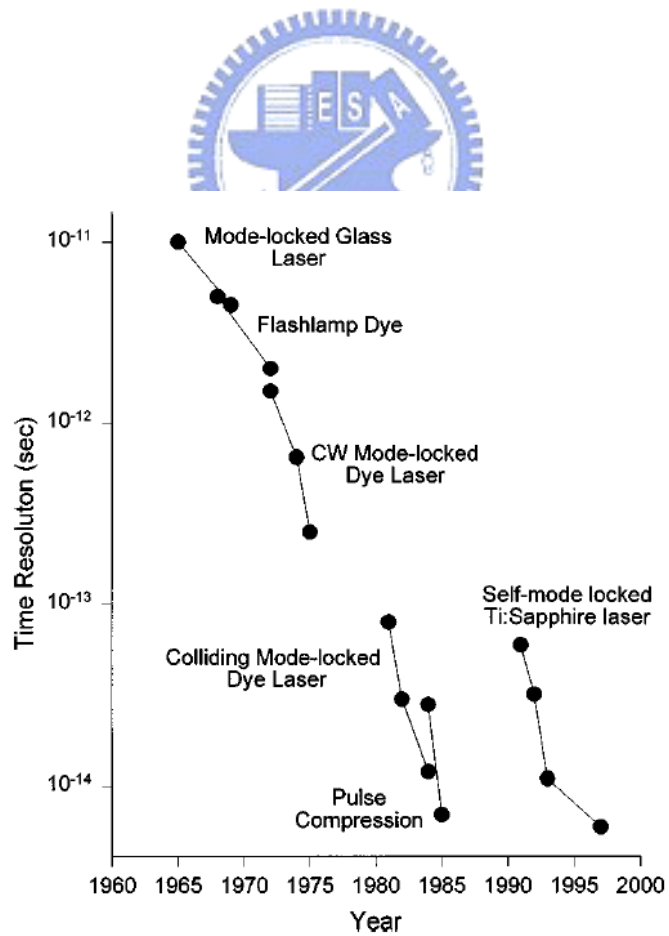


Fig. 1-4 Schematic diagram of the shortest pulses reported versus year. (Ref. 12)

Table 1-1 Fundamental processes in semiconductors.

Microscopic process	Characteristic time (s)
Carrier-carrier scattering	$10^{-15} \sim 10^{-12}$
Intervalley scattering	$>10^{-14}$
Intravalley scattering	$\sim 10^{-13}$
Carrier-optical phonon thermalization	$>10^{-12}$
Optical phonon-acoustic phonon interaction	$\sim 10^{-11}$
Carrier diffusion ($0.1 \mu\text{m}$)	$\sim 10^{-11}$
Auger recombination (carrier density 10^{20} cm^{-3})	$\sim 10^{-10}$
Radiative recombination	$>10^{-9}$
Lattice heat diffusion ($1 \mu\text{m}$)	$\sim 10^{-8}$

Table 1-2 List of the application of time-resolved spectroscopy.

Physics	<ul style="list-style-type: none"> ◦ Intraband & intersubband relaxation ◦ Phonon & Electron dynamics ◦ Energy gap dynamics ◦ Ionization dynamics ◦ Coherent polarization & population dynamics ◦ Laser-induced surface disordering ◦ Characterization of excited states dynamics ◦ Exciton dynamics
Chemistry	<ul style="list-style-type: none"> ◦ Solvent-solute interaction ◦ Polymer structure and dynamics ◦ Reaction kinetics in micelles ◦ Identification and detection of single molecule ◦ Electron and proton transfer ◦ Molecular vibration

Chapter 2 Femtosecond Time-Resolved Systems

The advantages in the generation of ultrashort laser pulses in the past decade have allowed realizing the long standing dream of probing ultrafast carrier dynamic directly in the time domain. The direct measurement of the temporal evolution of the scattering/relaxation processes with fs time-resolution has become possible. Several femtosecond time-resolved techniques will be described later.

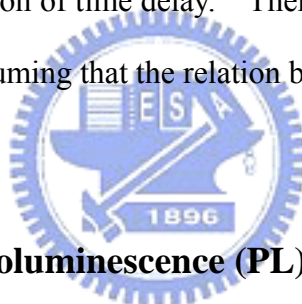
2.1 Pump-Probe Transmission/Reflection Spectroscopy

The most common adopted ultrafast spectroscopy technique is the pump-probe transmission/reflection technique. A schematic diagram of a generic pump-probe setup is shown in Fig. 2-1. The probe beam is typically much weaker than the pump, and the spot size of the probe at the sample is ideally considerably smaller than that of the pump so that it probes a region of uniform photoexcited density. For pump-probe transmission/reflection spectroscopy, one generally measures the change in the transmitted/reflected probe intensity induced by the pump as a function of the time delay between the pump and the probe pulses by chopping the pump beam and using a lock-in amplifier.

The principle of monitoring an ultrafast event by the pump-probe technique is illustrated in Fig. 2-2, where the pump and probe pulses are synchronized. For an event, $n(t)$, to be measured via pump-probe technique, its lifetime must not exceed the separating time between two pulses (13 ns in our case). The transmitted/reflected probe intensity from sample will vary with $n(t)$ while the probe pulses temporally overlapped with $n(t)$. However, this change due to $n(t)$ is very small, typically between $10^{-4} \sim 10^{-7}$, and is very difficult to detect directly under noisy

background (including laser noise, electronic noise, mechanic vibration etc.) by photodiode. Hence, the phase-lock technique was usually used to provide a background-free signal. The small signal was modulated by an optical chopper in order to eliminate the quite-large noise.

As noted, the modulation was commonly applied to the pump pulse train to make sure that the signal merely came from $n(t)$ induced by pump pulses. Then, the probe pulse train was also modulated by $n(t)$ on the constant intensity of the probe pulse train, i.e. a AC signal ($\Delta I(t)$) is added to a DC signal ($I_0(t)$). This signal was detected by the photodiode and fed to the lock-in amplifier, which was phase-locked to the optical chopper. By varying the time delay t between the pump and probe pulses, $\Delta I(t)$ would change as a function of time delay. Therefore, the temporal evolution of $n(t)$ could be measured by assuming that the relation between $n(t)$ and $\Delta I(t)$ is linear.

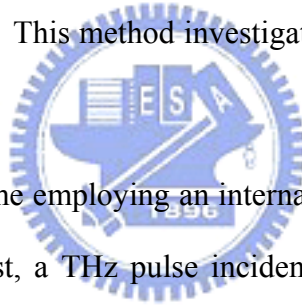


2.2 Time-Resolved Photoluminescence (PL) Spectroscopy

Time evolution of photoluminescence can also be obtained by scanning the relative delay between the two laser beams. The time-resolved PL technique is used not only to investigate carrier relaxation process, but also carrier transport process in semiconductors. The simplest method is to measure photoluminescence dynamics directly with a fast detector. The schematic diagram of time-resolved PL is shown in Fig. 2-1. The best technique for direct measurement is the used of streak cameras [14][15]. Two-dimensional streak cameras which provide spectral and temporal information simultaneously have become very attractive and versatile tools for the time-resolved PL Spectroscopy. Time-resolved photoluminescence spectra can also be obtained by keeping the delay fixed and scanning the angle of the sample. Some time-resolved PL experiment results of InGaAs(N) are discussed in Ref. [8][11][16].

2.3 Time-Resolved Terahertz-Probe Spectroscopy

Ultrafast lasers can generate coherent mm- and sub mm-wave radiation by a variety of different techniques. This radiation can be collimated and transmitted over reasonable distances, and can be detected using optically-gated photoconductive antennas. By adjusting the delay between the THz signal and the gating pulse, information about the amplitude and the phase of the THz signals can be obtained. The advantage of this technique by using an optical THz probe is that the THz probe photons have energy in the meV range and cannot substantially modify the electronic distribution in the sample. Thus the THz radiation propagates practically without absorption and dispersion in unexcited semiconductors and can detect even low concentrations ($\sim 10^{14} \text{ cm}^{-3}$). This method investigated in GaAs is discussed in Ref. [17][18][19].



A novel experimental scheme employing an internal reflection of the THz pulses is shown in Fig. 2-3 [20]. First, a THz pulse incident on the input surface is led to propagate through the sample in equilibrium. It is followed by the optical pump pulse, which generates free carriers near below the surface. The part of the THz pulse which passes through directly is not affected by the pump pulse and it is used as a reference. The part reflected on the output surface serves as a probe: It propagates back to the input surface, which has been excited meanwhile, and reflects from its inner side. Then, it can be detected as the echo, carrying a signature of the excited input surface (and equilibrium output surface).

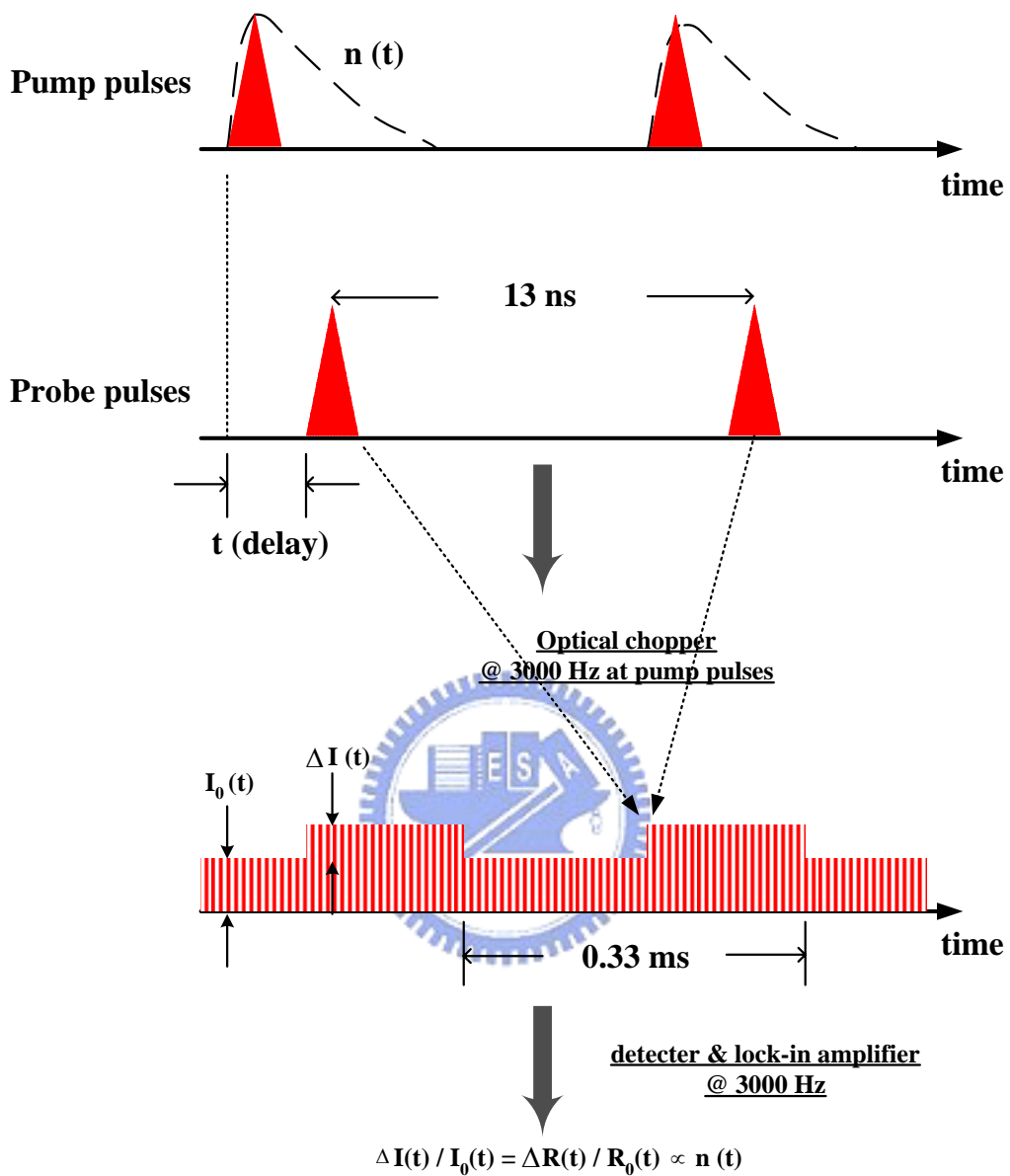


Fig. 2-2 The illustration for the principle of pump-probe technique.

Chapter 3 Ultrafast Spectroscopy of Semiconductor

3.1 Basic Concepts

3.1.1 Scattering Processes in Semiconductors

The dynamics of electrons, holes, excitons and phonons is influenced by their interaction with one another, as well as with defects and interfaces of the system. In the following subsections, we will discuss the various scattering mechanisms [21].

(a) Carrier-Phonon Interaction

Interaction of carriers with phonons plays a major role in the exchange of energy and momentum between carriers and the lattice, and hence determines the relaxation of photoexcited semiconductors. Optical phonon scattering and intervalley scattering are the most frequent of all the carrier-phonon scattering events. These processes always proceed on a picosecond time scale. On the other hand, acoustic phonon scattering of carriers is much less frequent than either optical phonon or intervalley scattering. The acoustic phonon processes take place on a nanosecond time scale.

(b) Carrier-Carrier Scattering

Carrier-carrier scattering determines the exchange of energy between carriers, and is primarily responsible for the thermalization of photoexcited non-thermal carriers. This process is mediated by Coulomb interaction and includes electron-electron, hole-hole and electron-hole scattering. The difference in the masses between electrons and holes reduces the energy change between these two species. The rate of carrier-carrier interactions can be found by using the Fermi golden rule of time-dependent perturbation theory.

The conditions under which carrier-carrier scattering has a significant effect on the photoexcited carrier distribution function can now be discussed. There are three conditions that must be satisfied. First the carrier-carrier scattering rates must be greater than the generation-recombination rates. Second, the exchanges of energy involved in carrier-carrier scattering should be greater than the energy exchanges in carrier-phonon scattering. Third, the carrier-carrier scattering rates should be greater than the carrier-phonon scattering rates.

3.1.2 Carrier Relaxation in Photoexcited Semiconductors

After a semiconductor is excited by an ultrashort pulse, it undergoes several stages of relaxation processes before it returns once again to the thermodynamic equilibrium [21]. The carrier relaxation can be classified into four temporally overlapping regimes :



(a) Coherent Regime

The laser pulse can create either real or virtual excitation. Excitations of a semiconductor created by an ultrashort laser pulse have well-defined phase relation within the excitation. This coherent regime exhibits many interesting phenomena which are elegant manifestations of basic quantum mechanics in semiconductors. The scattering processes that destroy the coherence are extremely fast in semiconductors and pico- and femtosecond techniques are required for studying the coherent regime in semiconductors.

(b) Non-thermal Regime

In the case of real excitation, the distribution of the excitation after the destruction of coherence through dephasing is very likely to be non-thermal, i.e. the distribution

function can not be characterized by a temperature. Investigation of this regime provides information about various processes, such as carrier-carrier or exciton-exciton scattering that bring the non-thermal distribution to a hot, thermalized distribution.

(c) Hot-Carrier Regime

Carrier-carrier or exciton-exciton scattering is primarily responsible for redistributing the energy within the carrier (exciton) system, and leads to a thermalized distribution function of carrier (exciton), i.e., a distribution that can be characterized by a temperature. The temperature is usually higher than the lattice temperature and may be different for different sub-systems (electrons, holes, or excitons). The thermalization time depends strongly on many factors such as carrier density. Investigation of this hot carrier regime focuses on the rate of cooling of carriers to the lattice temperature and leads to information concerning various carrier-phonon, exciton-phonon and phonon-phonon scattering processes.

(d) Isothermal Regime

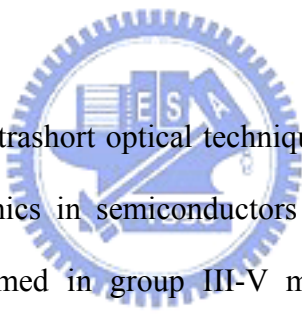
At the end of the hot-carrier regime, all the carriers are in equilibrium with each other, i.e., can be described by the same temperature of the lattice. However, there is still an excess of electrons and holes compared with the thermodynamic equilibrium. These excess electron-hole pairs recombine either radiatively or non-radiatively and return the semiconductor to the thermodynamic equilibrium.

These temporally-overlapping regimes are schematically illustrated in Fig. 3-1 with some typical processes that occur in each relaxation regimes. This time scale for each event depends very strongly on the excitation (free carrier vs. exciton), the density of excitation, and the lattice temperature and so on. It should be emphasized that many of the physical processes leading to relaxation in the different regimes are

occurring simultaneously. For example, the processes that destroy coherence may also contribute to thermalization of carrier distribution function, and emission of phonons may occur while the electron and holes are thermalizing to a hot distribution. The non-thermal carrier distribution function created by a femtosecond pulse is influenced by the dephasing of coherent polarization during the pulse. Nonetheless, this description in terms of four relaxation regimes does provide a convenient framework for describing and discussing the dynamics of relaxation in semiconductors.

3.2 Ultrafast Phenomena of Semiconductors

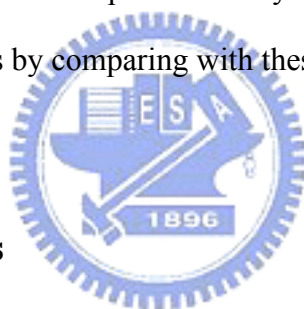
3.2.1 Bulk GaAs



Since the realization that ultrashort optical techniques allow the direct observation of carrier and phonon dynamics in semiconductors there have been an enormous amount of researches performed in group III-V materials. The direct bandgap characteristics of GaAs along with the availability of good quality samples had made GaAs the material of good choice in studying ultrafast carrier and phonon dynamics. Another reason for choosing group III-V as opposed to group IV materials is that the III-V materials were thought simpler to understand and to model due to their direct absorption and emission [12]. We will provide a brief description of the ultrafast spectroscopy of GaAs.

Time-resolved reflectance measurements with picosecond pulses were carried out by Auston *et al.* [22] in GaAs. From the experiments, Auston *et al.* deduced the rate of energy relaxation of hot electrons in GaAs to be approximately 0.4 eV/ps. A short time after Auston's experiments, Shank *et al.* [23] carried out some interesting

absorption measurement in GaAs. They reported on time-resolved absorption measurement in GaAs at 80 K, following an ultrashort laser pulse excitation. In 1988 Schoenlein *et al.* [24] investigated hot carrier dynamics in GaAs using the femtosecond pump and continuum probe technique. They observed spectral hole-burning due to a transient nonthermal carrier distribution and a rapid energy thermalization on a time scale of several tens of femtoseconds. Zhou *et al.* [25] used femtosecond luminescence to study ultrafast photoexcited holes in n-doped III-V compounds in 1992. The dynamics of electrons and holes were studied separately using n-doped samples and setting the excitation density much lower than the doping density. A number of investigations on the relaxation of photoexcited carriers of bulk GaAs have been reported in the past several years. We can easily discuss the carrier dynamics of bulk GaAs by comparing with these reports.



3.2.2 InGaAsN/GaAs

It has been discovered that a partial replacement of the column V elements with nitrogen leads to large changes in the material properties of group III-V compounds. The InGaAsN semiconductor has been intensively studied for its both fundamental properties and potential applications in the telecommunication field. Some experimental results of time-resolved measurements by other groups will give later.

In 1994, Sucha *et al.* [26] presented time-resolved measurements of carrier dynamics in bulk and quantum-well InGaAs using differential absorption spectroscopy. They found that the carrier thermalization time is 200-300 fs regardless of layer width for sample thickness ranging from 100 to 6000 Å. Borri *et al.* [27] studied the temperature and density dependences of exciton dephasing time in $\text{In}_{0.18}\text{Ga}_{0.82}\text{As}/\text{GaAs}$ single quantum well by the time-integrated four-wave mixing.

Bhattacharya *et al.* [28] performed pump-probe differential transmission spectroscopy on $\text{In}_{0.4}\text{Ga}_{0.6}\text{As}/\text{GaAs}/\text{AlGaAs}$ heterostructures.

Jiang *et al.* [8] investigated carrier dynamics in an $\text{In}_x\text{Ga}_{1-x}\text{As}_{1-y}\text{N}_y$ ($x\sim 0.03$, $y\sim 0.01$) epilayer grown on GaAs by MOCVD. Time-resolved photoluminescence (PL) measurement, performed for various excitation intensities and sample temperatures, indicates that the broad PL emission at low temperature is dominated by localized exciton recombination. Grenouillet *et al.* [29] reported an anomalous temperature dependence of the PL spectrum of a 7 nm $\text{InGaAsN}/\text{GaAs}$ single quantum well. Kaschner *et al.* [10] investigated the recombination process in $\text{InGaAsN}/\text{GaAs}$ multiple quantum wells by time-resolved measurements.

Tansu *et al.* succeeded in developing several dilute-nitride quantum well (QW) on GaAs substrate by metal-organic chemical vapor deposition (MOCVD) in the past few years. These high-performance InGaAs(N) QW lasers have been realized with lasing performance up to emission wavelength of 1233 – 1300 nm [30][31][32]. Their temperature dependent PL can be found in Ref. [33]. Carrier recombination was investigated from the behavior of the differential carrier lifetime with carrier density on two $\text{InGaAs}_{1-x}\text{N}_x$ single quantum well laser diodes, that differ only in the nitrogen content x in the well [7]. It is shown that the recombination lifetime is significantly reduced when nitrogen is added into the QW. In CLEO 2005, these samples were reported that a quantum-dot like behavior and a strong localization affect the carrier dynamics for temperature from 15 to 150 K by time-resolved PL [34]. The interesting behaviors in III-V-N compounds are full of vitality studied at present.

3.3 Carrier-Induced Change in Refractive Index

3.3.1 Band Filling

The electrons and holes as Fermions can occupy each quantum state only once according to the Pauli exclusive principle. Hence each k state in a semiconductor band can be occupied twice, once with a spin-up and once with a spin-down carrier. An occupied state is no longer available as a final state in an optical absorption process. Due to the principle of energy minimization, the carriers in quasi-equilibrium occupy the available states from the bottom of the band, so that the energetically lowest states are occupied first. This results in filling the states near the bottom of the conduction band by electrons and the top of the valance band by holes. Hence, there is a decrease in the absorption coefficient at energies above the bandgap.

If parabolic bands are assumed or under the effective-mass approximation, the optical absorption near the bandgap in a direct-gap semiconductor is given by the square-root law: $\alpha_0(E) = \frac{C}{E} \sqrt{E - E_g}, E \geq E_g$ and $\alpha_0(E) = 0, E \leq E_g$, where $E = \hbar\omega$ is the photon energy, E_g is the bandgap energy, and C is a constant involving material's parameters, matrix elements between periodic parts of the Bloch states at the band edges, and the fundamental constants.

In the case of band filling, there is a finite probability that a state in the conduction band will be occupied by an electron and/or a state in the valance band will be empty (of electrons). If we denote an energy in the valance band by E_a and an energy in the conduction band by E_b , then the absorption coefficient of an injected semiconductor is $\alpha(N, P, E) = \alpha_0(E)[f_v(E_a) - f_c(E_b)]$. Here N and P are the concentrations of free electrons and holes, respectively, α_0 represents the absorption of

pure materials in the absence of injection, $f_c(E_b)$ is the probability of a conduction band state of energy E_b being occupied by an electron, and $f_v(E_a)$ is the probability of a valance band state of energy E_a being occupied by an electron. The change in absorption induced by the band filling is $\Delta\alpha(N, P, E) = \alpha_0(E)[f_v(E_a) - f_c(E_b) - 1]$. For the case of injection, we will have $f_c > 0$ and $f_v < 1$ close to the respective band edges. This formula predicts $\Delta\alpha$ is negative, i.e., the band filling decreases the absorption coefficient at a fixed incident photon energy.

The real and imaginary parts of the refractive index $n + i\kappa$ (or of the dielectric constant $\varepsilon_1 + i\varepsilon_2$) are not independent. They are related by the Kramers-Kronig integrals $n(E) = 1 + \frac{2c\hbar}{e^2} P \int_0^\infty \frac{\alpha(E')}{E'^2 - E^2} dE'$, where $\alpha = \frac{4\pi\kappa}{\lambda}$, c is the speed of light, e is the electron charge, E is the photon energy, and P indicates the principal value of the integral. In analogy with the change of absorption coefficient we defined $\Delta n(N, P, E) = n(N, P, E) - n_0(E)$, where n_0 is the refractive index of uninjected material. The change in refractive index is then given by $\Delta n(N, P, E) = \frac{2c\hbar}{e^2} P \int_0^\infty \frac{\Delta\alpha(N, P, E')}{E'^2 - E^2} dE'$. The refractive index decreases for energies near and below E_g , and Δn becomes positive for energies well above E_g .

3.3.2 Bandgap Renormalization

A consequence of the Coulomb interaction among the laser-excited electronic excitations is the effect of the bandgap skrinkage (bandgap renormalization); i.e., the energies of the electrons and holes in their respective bands are reduced. This energy reduction is a consequence of the exchange effect for particles with equal spin, and Coulomb correlation effect for all particles. The exchange effect is caused by the Pauli exclusive principle. The probability that two Fermions with identical

quantum numbers are at the same point in real space is zero. For increasing separation between the particles, the probability slowly approaches unity. Hence, the Pauli exclusion leads to a reduction of the probability that equally charged particles come close to each other, and this in turn reduces the repulsive (i.e., positive Coulomb energy) contribution.

An expression for the bandgap renormalization, originally derived by Wolff, is $\Delta E_g = -\left(\frac{e}{2\pi\epsilon_0\epsilon_s}\right)\left(\frac{3n_{eh}}{\pi}\right)^{1/3}$, where n_{eh} is the concentration of free electrons or holes, ϵ_0 is the permittivity of free space, and ϵ_s is the relative static dielectric constant of the semiconductor. The estimated shrinkage is proportional to the cube-root of the carrier concentration or the average interparticle spacing. We modeled the bandgap renormalization to cause a rigid translation (red shift) of the absorption curve. The change in absorption due to bandgap renormalization is predicted to be $\Delta\alpha(n_{eh}, E) = \frac{C}{E}\sqrt{E - E_g - \Delta E_g(n_{eh})} - \frac{C}{E}\sqrt{E - E_g}$. It predicts $\Delta\alpha$ which is always positive, the largest near the bandgap, and rapidly decreasing for higher energies. As with band filling, the change in refractive index was calculated by applying the Kramers-Kronig integral to the $\Delta\alpha$ from bandgap renormalization, the largest change in refractive index is near the bandgap. Unlike band filling, however, the bandgap renormalization causes negative change in refractive index ($\Delta n < 0$) for energies above the bandgap as a result of decreasing in absorption coefficient for a fixed incident photon energy.

3.3.3 Free-Carrier Absorption

Thus far, we have considered changes of the interband absorption due to band filling and bandgap renormalization effects. In addition, a free carrier can absorb a photon and move to a higher energy state within a band. In the Drude model, this intraband free carrier absorption, also known as the plasma effect, is modeled as being directly proportional to the concentration of electrons and holes and the square of the wavelength. The corresponding change in refractive index is given by $\Delta n = -\left(\frac{e^2 \lambda^2}{8\pi^2 c^2 \epsilon_0 n}\right)\left(\frac{N}{m_e} + \frac{P}{m_h}\right)$, where λ is the photon wavelength, m_e is the effective mass of electrons, and $\frac{1}{m_h} = \frac{m_{hh}^{1/2} + m_{lh}^{1/2}}{m_{hh}^{3/2} + m_{lh}^{3/2}}$ with m_{hh} and m_{lh} being the effective masses of heavy holes and light holes, respectively. The sign of Δn from the plasma effect is always negative. Hence, the change of reflectance ΔR in pump probe measurement is negative.



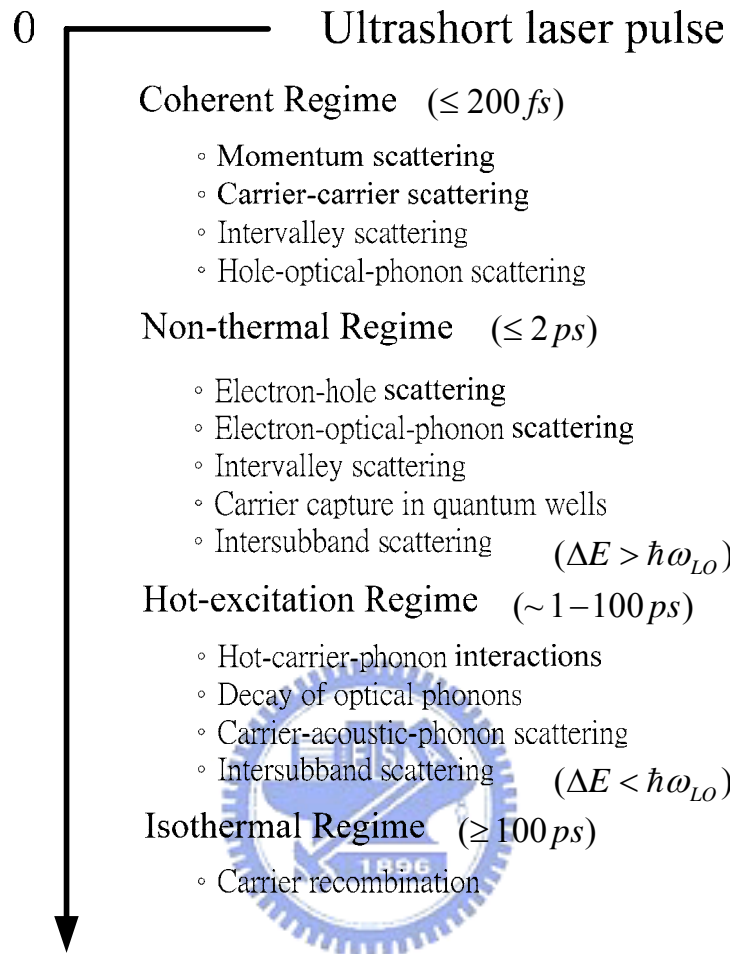


Fig. 3-1 Four temporally overlapping relaxation regime in photoexcited semiconductors.

Chapter 4 Experiments

4.1 InGaAsN Single Quantum Well Structures

The investigated samples were grown by low-pressure metalorganic chemical vapor deposition (LP-MOCVD) by Tansu et al. Trimethylgallium, trimethylaluminium, and trimethylindium are used as the group-III sources. The group-V precursor used here are AsH₃ and PH₃, and the N precursor was U-dimethylhydrazine. The dopant sources are SiH₄ and diethylzinc for the n and p dopants, respectively. The active regions are all based on the 60Å In_{0.4}Ga_{0.6}As_{1-x}N_x QW, sandwiched with various barrier materials. The In and N contents of the InGaAsN material were determined from high-resolution x-ray diffraction and secondary mass ion spectroscopy. The N composition x in the structures is 0% and 0.5% for samples A and B, respectively. The schematic diagrams of the structure investigated here are shown in Fig. 4-1 [30]. The details of growth optimization can be found in Ref. [30][30][31].

High resolution transmission electron microscopy (HRTEM) image shown in Fig. 4-2 is performed for the interface quality of In_{0.4}Ga_{0.6}As_{0.995}N_{0.005}/GaAs SQW [33]. The crystal quality and interface of quantum are directly investigated. The rough interface shows a deteriorated material quality, compared with the conventional III-V materials. The room-temperature PL spectra of the samples are presented in Fig. 4-3. The band gap of these samples are 1.04eV (1.2µm) and 0.97 eV (1.3µm) for In_{0.4}Ga_{0.6}As and In_{0.4}Ga_{0.6}As_{0.995}N_{0.005} SQW, respectively.

4.1.1 Mode-Locked Ti:sapphire laser

A commercial Kerr-lens-mode-locked Ti:sapphire laser (Coherent Mira900) is used as the light source. Typically, the pulse width is 175 fs and the pulse repetition rate is 75 MHz and the wavelength is tunable from 700 nm to 900 nm. Fig. 4-4 shows the optical path within the laser cavity. The Ti:sapphire laser is pumped by a diode-pumped frequency-doubled Nd:YVO₄ laser (Coherent Verdi-8). The pump power is 8 W (?) and the output power is smaller than 1 W.

4.1.2 Autocorrelator

Autocorrelation measurement using second harmonic generation (SHG) is the most common method for measuring the pulse-width of ultrashort laser pulse. A schematic of intensity autocorrelator is shown in Fig. 4-5. The laser beam is split into two with identical power by 50/50 beamsplitter. One beam is temporally delayed by a translation stage. Two beam focus non-collinearly onto a beta barium borate (BBO) nonlinear optical crystal. The autocorrelation signal comes from the second harmonic generation (SHG) of BBO is detected by a silicon detector. The signal is then recorded on a personal computer. The result of the autocorrelation trace is shown in Fig. 4-6. The red curve is the Gaussian fit to the data. The measured pulse-width of our laser is 230 fs.

4.1.3 Experimental Setup of Femtosecond Time-Resolved

Measurement

Figure 4-7 shows the schematic diagram of the femtosecond time-resolved setup.

The ultrafast time-resolved photorefectance experiments are performed at room temperature using the pulsed Ti:sapphire laser described in Sec.4.2.1. The laser beam is split into pump and probe beams by 50/50 beamsplitter (BS). The variable neutral density filter (ND1) is used to attenuate the power of probe beam to keep the pump probe ratio 20:1. Another variable neutral density filter (ND2) is used to adjust the power of the pump beam. The 1.25 μm -stepping resolution translation stage, controlled by a computer, is used to change the optical path length of the pump beam, resulting in a (positive or negative) time delay between the pump and the probe pulses. The minimal time delay is 8.33fs. In order to minimize the optical coherent artifacts, the polarization of the pump beam is rotated perpendicularly to that of probe beam by a half-wave ($\lambda/2$) plate. The pump and probe beams then are focused separately by two identical convex lenses with focal length 10 cm and 5 cm. The focused pump beam spot size $\sim 250 \mu\text{m}$. The spatial overlap of pump and probe beams on the sample was monitored by a CCD camera. The reflected pump beam is rejected using an iris. A silicon photodetector (Newport 818-SL series) detects the reflected intensity of the probe beam. With an optical chopper in the pump beam path, the detected signal is processed with a lock-in amplifier (Stanford Research System, Model SR830) to perform a phase locked measurement. The probe is then recorded on a personal computer as a function of temporal delay between pump and probe beams.

4.1.4 Zero Delay point

In this experiment, it is important to find out the zero-delay point ($\Delta t=0$). In order to find out the zero point, we focused the laser pulses into a beta barium borate (BBO) crystal to produce frequency-doubled visible light. The type-I phase matching

condition of second harmonic generation (SHG) is given by $\Delta k = k(\omega_2) - 2k(\omega_1) = 0$,
 where $k(\omega_1) = \frac{2\pi n_1(\omega_1)}{\lambda_1}$, $k(\omega_2) = \frac{2\pi n_2(\omega_2)}{\lambda_2}$, $\lambda_1 = 2\lambda_2$, and
 $n_2(\omega_2) = n_e(\omega_2, \theta) = \left(\frac{\cos^2 \theta}{n_o^2(\omega_2)} + \frac{\sin^2 \theta}{n_e^2(\omega_2)} \right)^{-1/2}$, respectively. Here, θ is the phase
 matching angle, ω_1 is the fundamental angular frequency, $\omega_2 = 2\omega_1$, n_o is the ordinary
 refractive index, and n_e is the extra-ordinary refractive index.



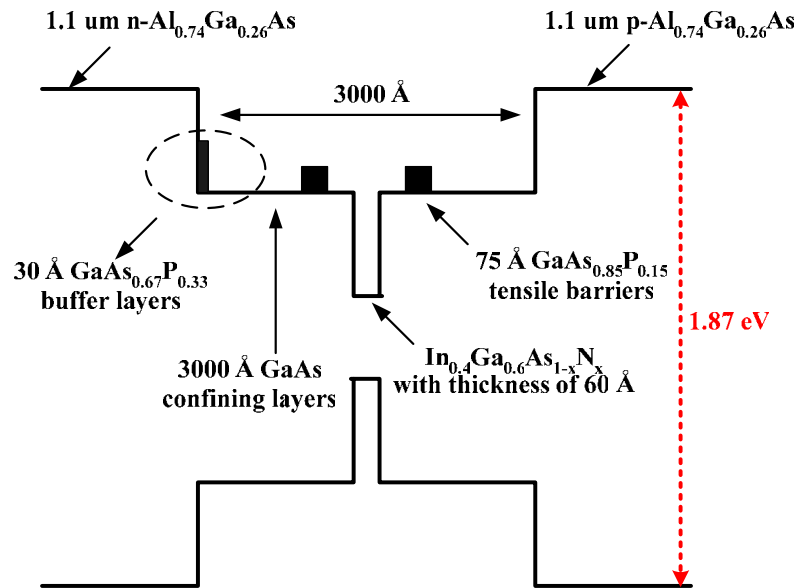


Fig. 4-1 Cross-sectional schematic conduction band diagram of the $\text{In}_{0.4}\text{Ga}_{0.6}\text{As}_{1-x}\text{N}_x$ SQW (Ref. [30]).

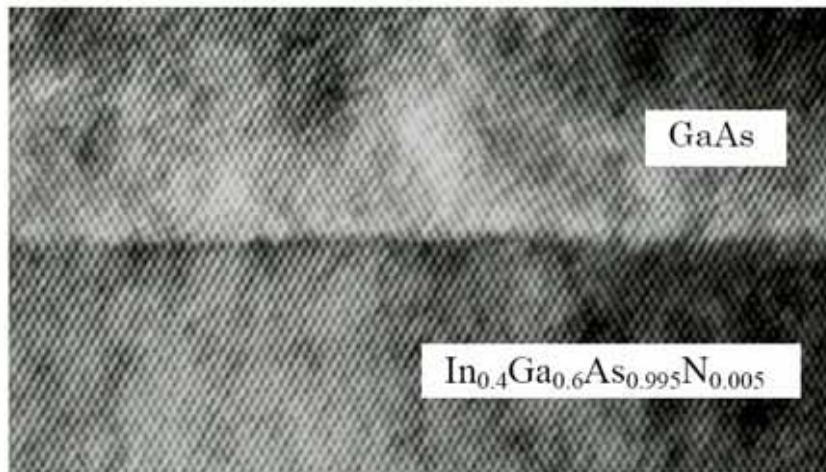


Fig. 4-2 HRTEM image of $\text{In}_{0.4}\text{Ga}_{0.6}\text{As}_{0.995}\text{N}_{0.005}/\text{GaAs}$ SQW (Ref. [33]).

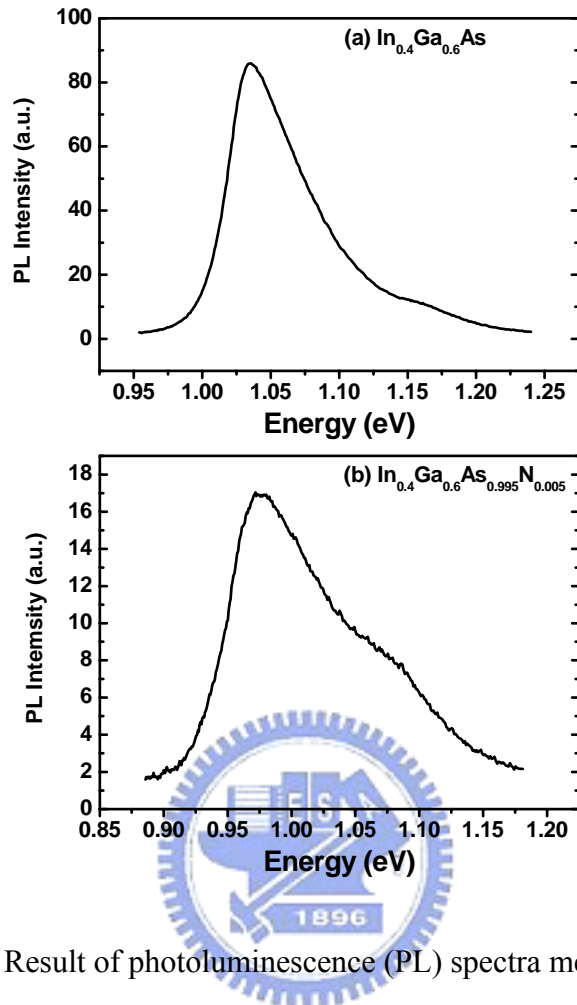


Fig. 4-3 Result of photoluminescence (PL) spectra measurement.

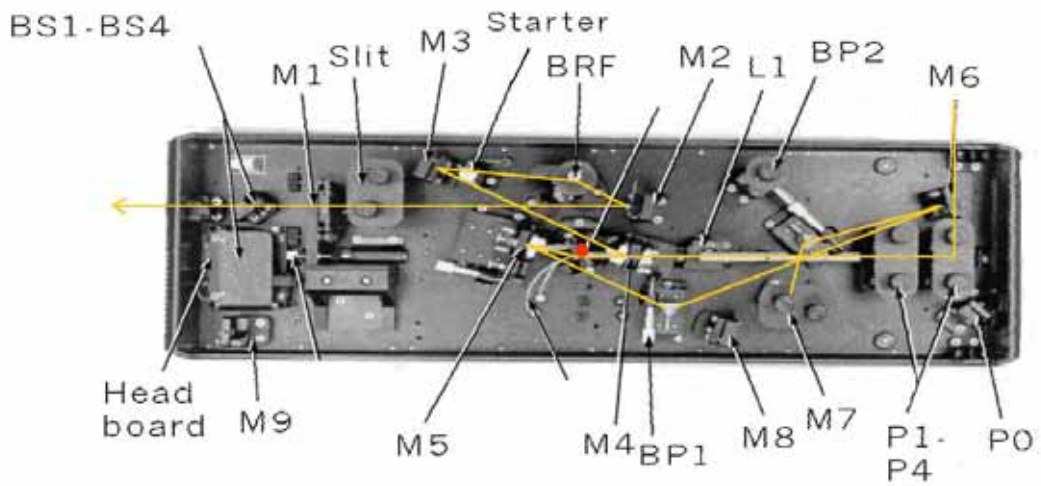


Fig. 4-4 The optical beam path within Coherent Mira-900.

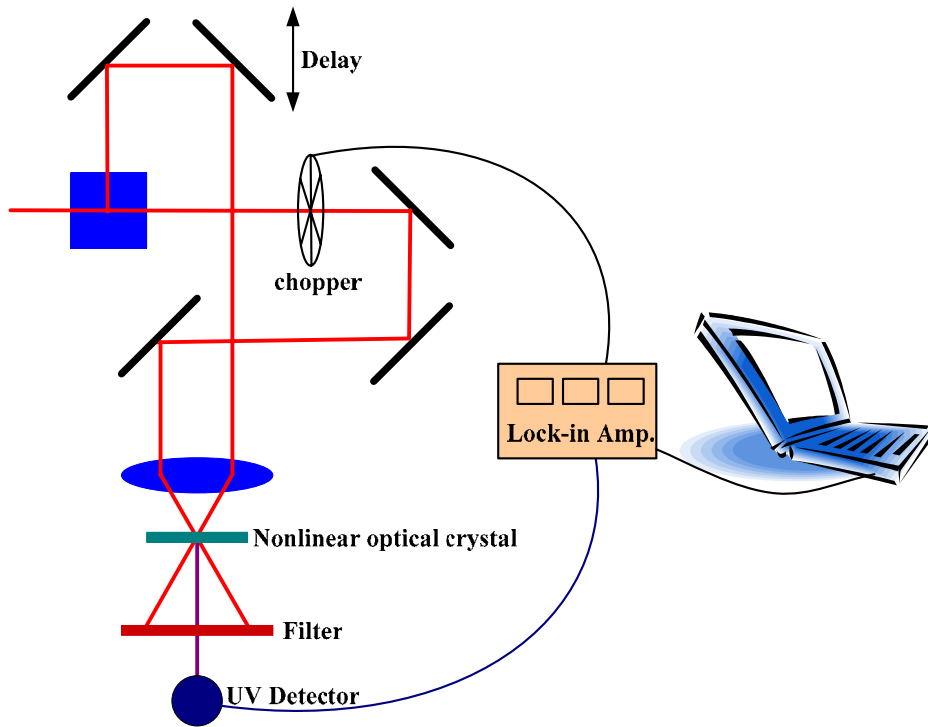


Fig. 4-5 Sketch diagram of the intensity autocorrelator.

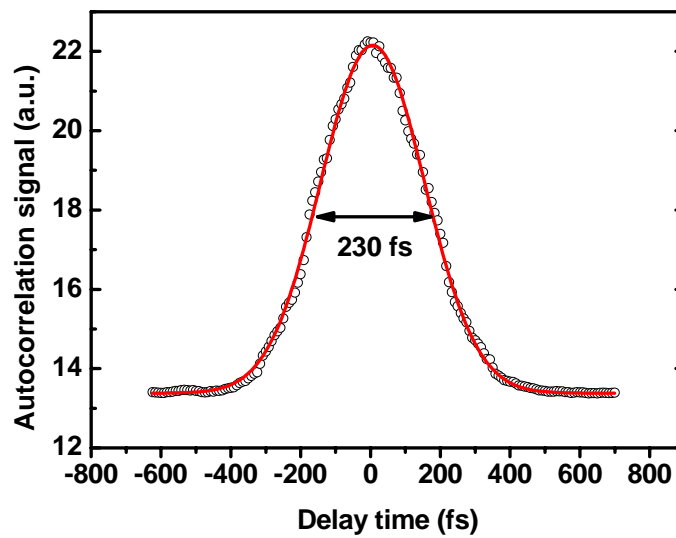


Fig. 4-6 The autocorrelation trace.

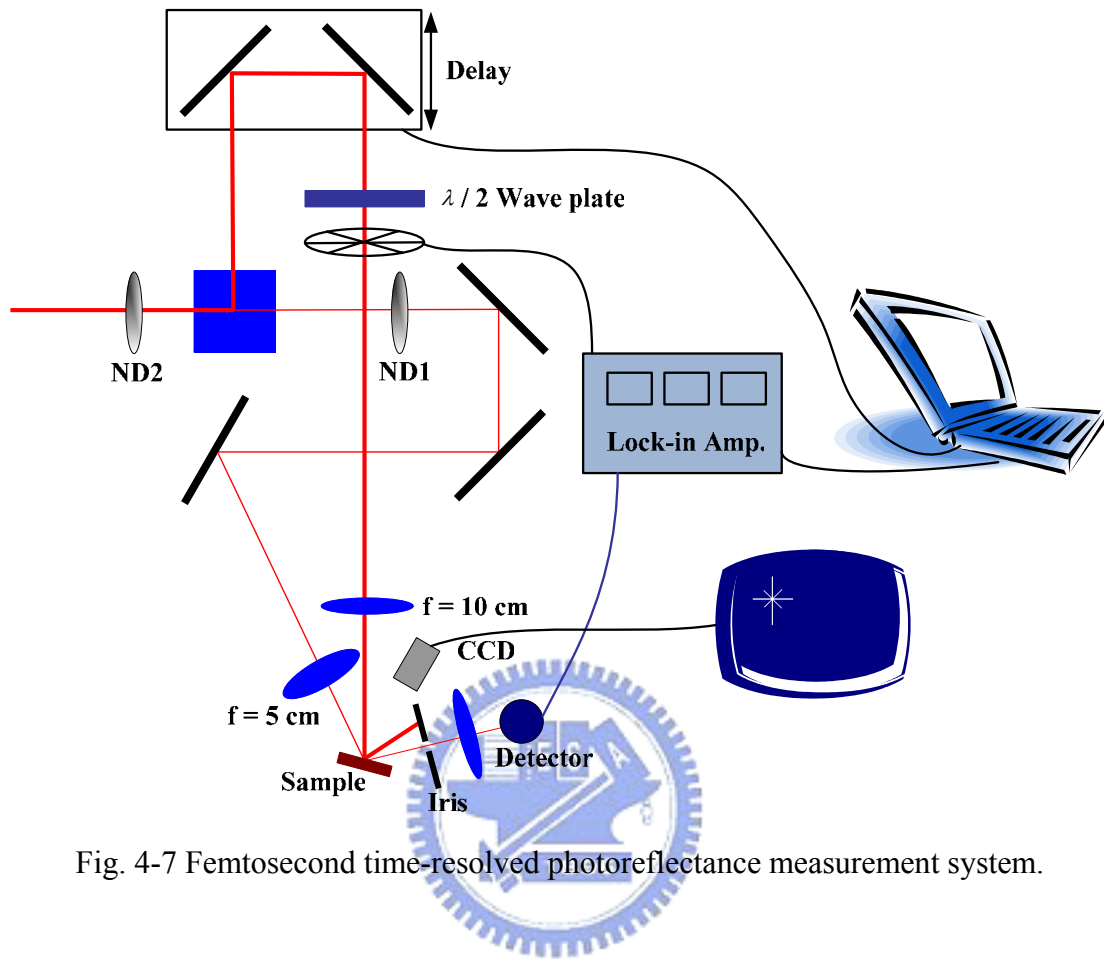


Fig. 4-7 Femtosecond time-resolved photoreflectance measurement system.

Chapter 5 Results and Discussion

The time-resolved photorefectance response of the semiconductor to optical pulses can be broadly attributed to the effects of the carriers generated by the pump pulses via interband transition. The change in the complex dielectric function induced by these carriers is governed by the various carrier relaxation and decay mechanisms inside the semiconductor. This essentially determines the reflectivity of the probe pulse. This change can be modeled by considering the absorption change due to band filling (BF), the band gap shift due to the presence of carriers (better known as band-gap renormalization or BGR), plasma screening effect, enhancement of absorption due to the Coulomb enhancement factor (CEF), and intraband absorption of photons by the free carriers (FCA).

The change in the reflectivity is due to the change in the complex refractive index $(n + i\kappa)$. In general, the major contributions to the change in n can be written as $\Delta n = \Delta n_{BF+BGR} + \Delta n_{FCA}$. The change in the reflectivity (ΔR) which is the difference between the reflectivity R with the pump ON and the pump OFF, can be calculated as $\Delta R(h\nu) = R(n', \kappa', h\nu) - R(n, \kappa, h\nu)$. Here the reflectivity $R(n, \kappa, h\nu)$ is given by $R(n, \kappa, h\nu) = \frac{[n(h\nu) - 1]^2 + \kappa^2(h\nu)}{[n(h\nu) + 1]^2 + \kappa^2(h\nu)}$, and κ is related to α by the relation $\kappa(h\nu) = \frac{\lambda}{4\pi} \alpha(h\nu)$ and $\Delta\kappa(h\nu) = \frac{\lambda}{4\pi} \Delta\alpha(h\nu)$. The values of n' and κ' are the modified real and imaginary parts of refractive index, respectively, in the presence of the carrier density N (or in the presence of the pump beam, i.e. pump-ON condition).

We will show our results of bulk GaAs and InGaAsN/InGaAs SQWs in the followings.

5.1 Ultrafast Time Resolved Photoreflectance of Bulk GaAs

Figure 5-1 shows the experimental result for bulk GaAs pumped at 800 nm (or photon energy 1.55eV) with various pump power. Initially, a fast positive peak was observed and then it follows a long tail. The physical reason for the fast positive peak is absorption bleaching. The rising is due to the generation of carriers occupying the optical-coupled transition states. As a result, the real part of the complex refractive index increases at frequencies which are high compared with the probing frequency and hence the reflectance increases. The decay is due to carrier being scattered out of their initial states and subsequent relaxation toward the band edges through carrier-carrier scattering and carrier-phonon scattering. In GaAs, the carrier-carrier scattering time of 30 fs were observed with carrier density of 10^{17}cm^{-3} [35]. In our experimental condition, 230 fs pulses used in Fig. 5-1, the carrier-carrier scattering process may not be time-resolved [36]. Therefore, the decaying of the transient is attributed to cooling of hot carriers by emitting LO phonons. Since the carrier-phonon scattering rate in semiconductor is independent of carrier density, the decay rate of the transient is expected to be constant at different excitation densities [21].

The pump intensities of Fig. 5-1 vary from 0.29–2.9 MW/cm². At the pump wavelength (800 nm or 1.55 eV), the absorption coefficient of GaAs is about $1.5\ \mu\text{m}^{-1}$ [37]. The corresponding peak excitation densities are estimated to be 0.4×10^{15} – $4.04 \times 10^{16}\ \text{cm}^{-3}$. The excess energy of initial carriers is 0.13 eV for each electron-hole (e-h) pair with bandgap of 1.42 eV for GaAs. For a LO phonon energy of 37 meV in GaAs, each hot electron emits 3 LO phonons in cascade before reaching the band edge [38].

In Fig. 5-2 we found that the peak amplitude of ΔR does increase with increasing

pump power. It is proportional to the carrier density at low pumping due to the band filling effect, but it becomes flattened even slightly decreases with increasing pump power at high pumping. The magnitude of ΔR peak is proportional to the density of carriers accumulated in the allowed optical transition states after photoexcitation. At high pumping, the rate of carrier-carrier scattering becomes faster due to more carriers being generated [35]. As a result, the injection carriers cause a bandgap shrinkage by the bandgap renormalization, which is given by $\Delta E_g = -\left(\frac{e}{2\pi\epsilon_0\epsilon_s}\right)\left(\frac{3n_{eh}}{\pi}\right)^{1/3}$ [39], where n_{eh} is the e-h pair density in cm^{-3} , ϵ_0 is the permittivity of free space, and ϵ_s is the static dielectric constant of the semiconductor (12.9 in bulk GaAs [40]). The renormalized bandgaps are estimated to be 1.415 eV and 1.412 eV, for 10 mW and 100 mW pumping, respectively. For a fixed photon energy, as the bandgap becomes narrower, the range of allowed optical transition states would be enlarged, which in turn reduces the state-filling (band-filling) effect. Therefore, at high pumping, the nonlinear relation between the peak amplitude of ΔR and the injected carrier density is due to the enhance carrier-carrier scattering and the induced bandgap shrinkage to decrease ΔR .

The normalized ΔR traces with various pump powers are shown in Fig. 5-3. To extract the carrier lifetime, we fitted the experimental ΔR traces (starting from the delay time; in most cases, 233 fs from the peak of the trace) by a double exponential decay function, $A\exp(-t/\tau_1) + B\exp(-t/\tau_2)$. By varying parameters A, B, τ_1 , and τ_2 , we can obtain the best fit to the data (Appendix I). The carrier lifetime versus pump power is shown in Fig. 5-4. The fast component of carrier lifetime approximates 0.2 ± 0.04 ps, and it is not change with increasing pump intensity. This result confirms that the carrier relaxation is due to electron-phonon scattering [21]. The slow component of carrier lifetime approximates 2.15 ps, resulting from the

cooling of the hot carrier distribution to the lattice temperature [36][41].

5.2 Ultrafast Time Resolved Photoreflectance of InGaAs_{1-x}N_x SQW

Figure 5-5 shows the ultrafast time-resolved photoreflectance of In_{0.4}Ga_{0.6}As SQW and In_{0.4}Ga_{0.6}As_{0.995}N_{0.005} SQW with pump power of 10–50 mW at 800 nm. Although the thickness of the SQWs is only 6 Å within a 3000 Å wide confining layer (GaAs), we still can find quite different photoreflectance results of In_{0.4}Ga_{0.6}As SQW and In_{0.4}Ga_{0.6}As_{0.995}N_{0.005} SQW. The negative change of transient reflectance corresponds to the negative index change on the order of 10⁻⁵ – 10⁻⁴ for In_{0.4}Ga_{0.6}As SQW. This is evaluated by using the simplified Kramers-Kronig relation (Esser *et al.* 1990) to be $\frac{\Delta R}{R} \approx \frac{4}{(n^2 - 1)} \Delta n$. Here n is 3.43 of In_{0.4}Ga_{0.6}As SQW [42]. The mechanism of negative change of transient reflectance is very complicated and still does not fully understand at present. Bandgap renormalization, free-carrier absorption (FCA) or re-excitation of trapped carriers into the conduction band may account for the negative change of transient reflectance [43].

The measured peak amplitude of ΔR versus pump power is shown in Fig. 5-6. The peak amplitude of ΔR increases linearly with the pump intensity. The magnitude of ΔR peak, which in In_{0.4}Ga_{0.6}As SQW is larger than in In_{0.4}Ga_{0.6}As_{0.995}N_{0.005} SQW, is determined by the population of carriers accumulated in the allowed optical transition states after photoexcitation. In comparison, the carrier lifetimes of In_{0.4}Ga_{0.6}As_{0.995}N_{0.005} SQW are shorter than those of In_{0.4}Ga_{0.6}As SQW. This is also found in the time-resolved PL measurements by Lifang *et al.* [34] and the below threshold modulation frequency response measurements by Anton *et al.* [7].

Using a single exponential decay function, $A \exp(-t/\tau_1)$, the fitting results are shown in Appendix II. We can see that they do not quite match with our measurement results. So we fit the normalized ΔR traces of $\text{In}_{0.4}\text{Ga}_{0.6}\text{As}$ and $\text{In}_{0.4}\text{Ga}_{0.6}\text{As}_{0.995}\text{N}_{0.005}$ SQWs with various pump power by a double exponential decay function again (see Appendix III). List of carrier lifetimes of $\text{In}_{0.4}\text{Ga}_{0.6}\text{As}$ SQW and $\text{In}_{0.4}\text{Ga}_{0.6}\text{As}_{0.995}\text{N}_{0.005}$ SQW with various pump power given in Table 5-1. In order to explain both the smaller nonlinearity and the carrier lifetimes we suggest that defects are created with N incorporation. These defects form trap states within the bandgap. These trap states very efficiently capture excited carriers and act as nonradiative recombination centers. This capture takes place in a shorter time scale than the intraband relaxation, thus explaining the comparably shorter carrier lifetimes. Because of the localized nature of these traps, even carriers in excited states above the conduction band minimum can be captured. Unpredictably, such thin SQW of only 6 Å within a 300 Å wide confining layer, this effect is sensitive enough to contribute to the small maximum reflectivity changes of $\text{In}_{0.4}\text{Ga}_{0.6}\text{As}_{0.995}\text{N}_{0.005}$ SQW as compared to $\text{In}_{0.4}\text{Ga}_{0.6}\text{As}$ SQW. In addition, the band gap renormalization effect decreases the band filling effect. Similar results of negative ΔR and lifetime shortening due to defect trapping had been reported for low-temperature grown GaAs (LT-GaAs), in which defects (As antisites) form efficient nonradiative recombination centers as compared with bulk GaAs.

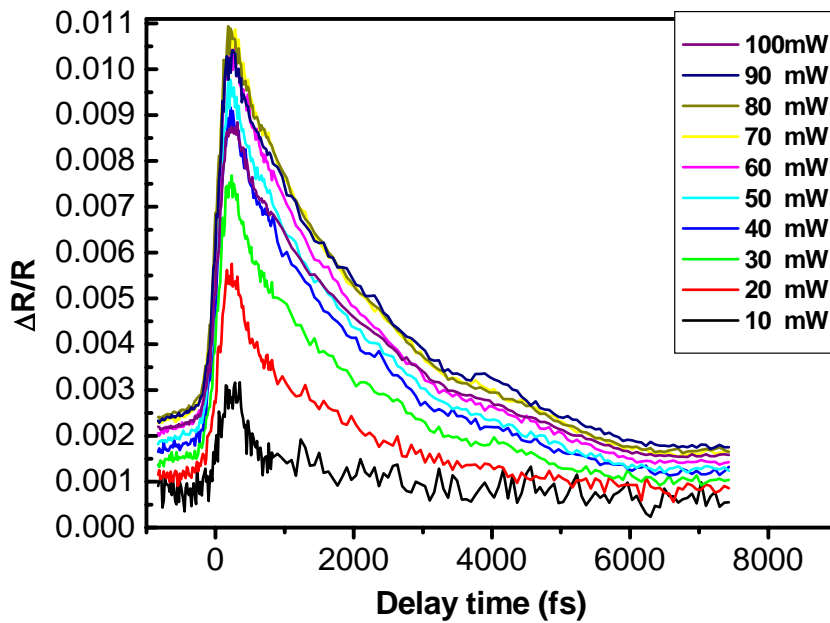


Fig. 5-1 Pump-intensity dependent time-resolved photorefectance of bulk GaAs.

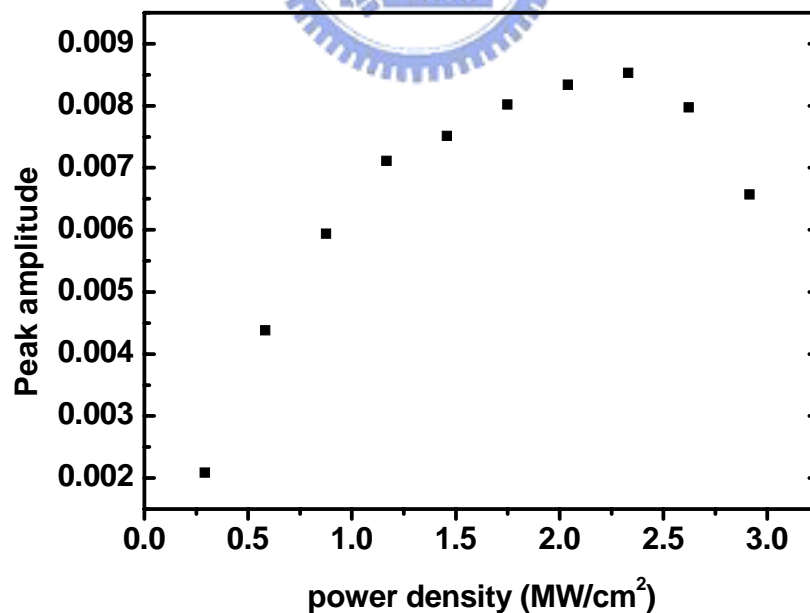


Fig. 5-2 The measured ΔR peak amplitude versus pump power in bulk GaAs.

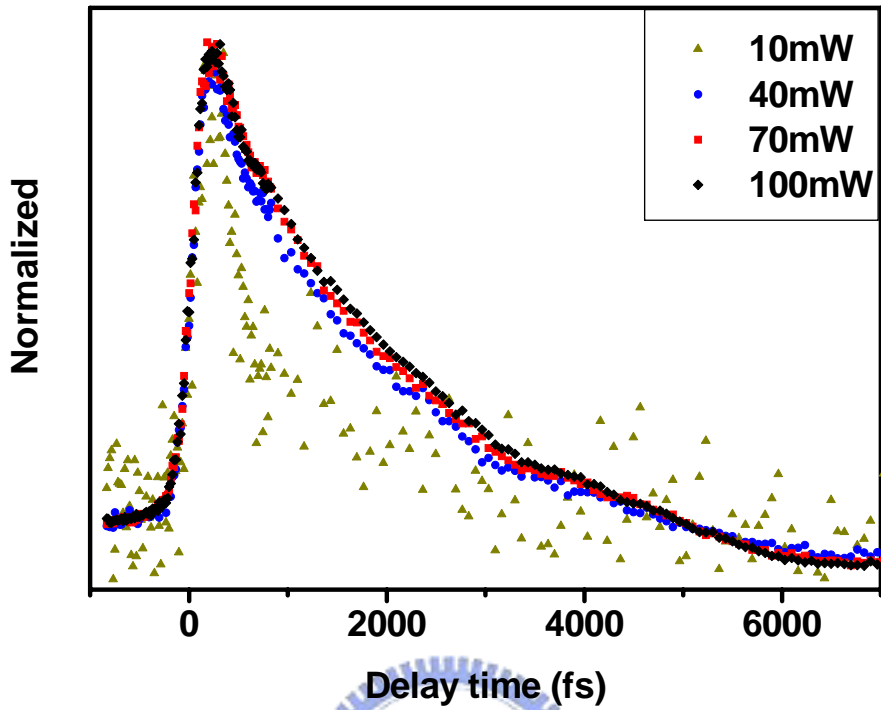


Fig. 5-3 The normalized ΔR traces of bulk GaAs with various pump power.

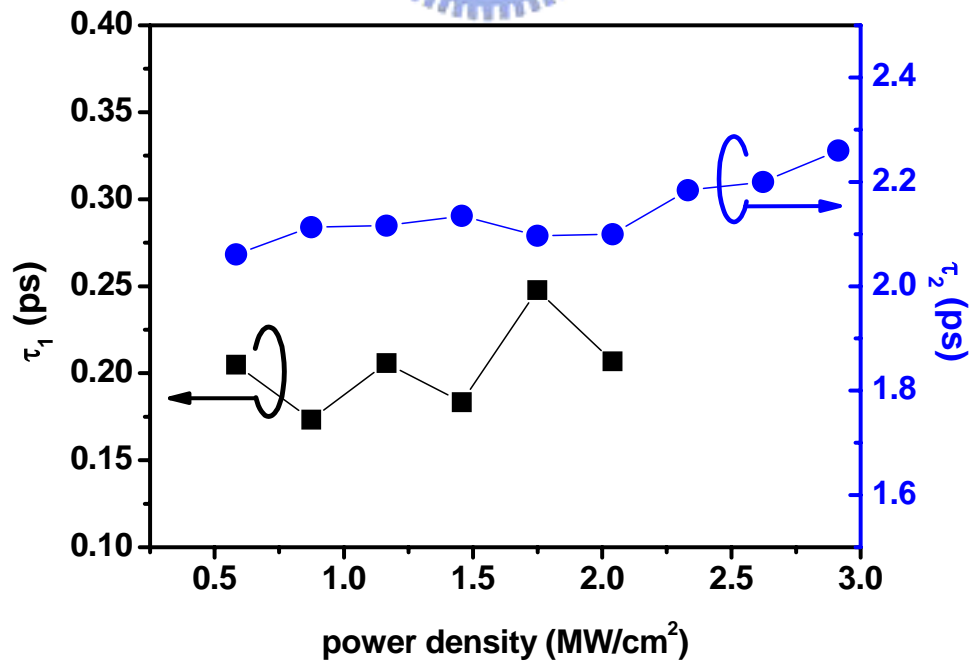


Fig. 5-4 The carrier lifetime versus pump power in bulk GaAs.

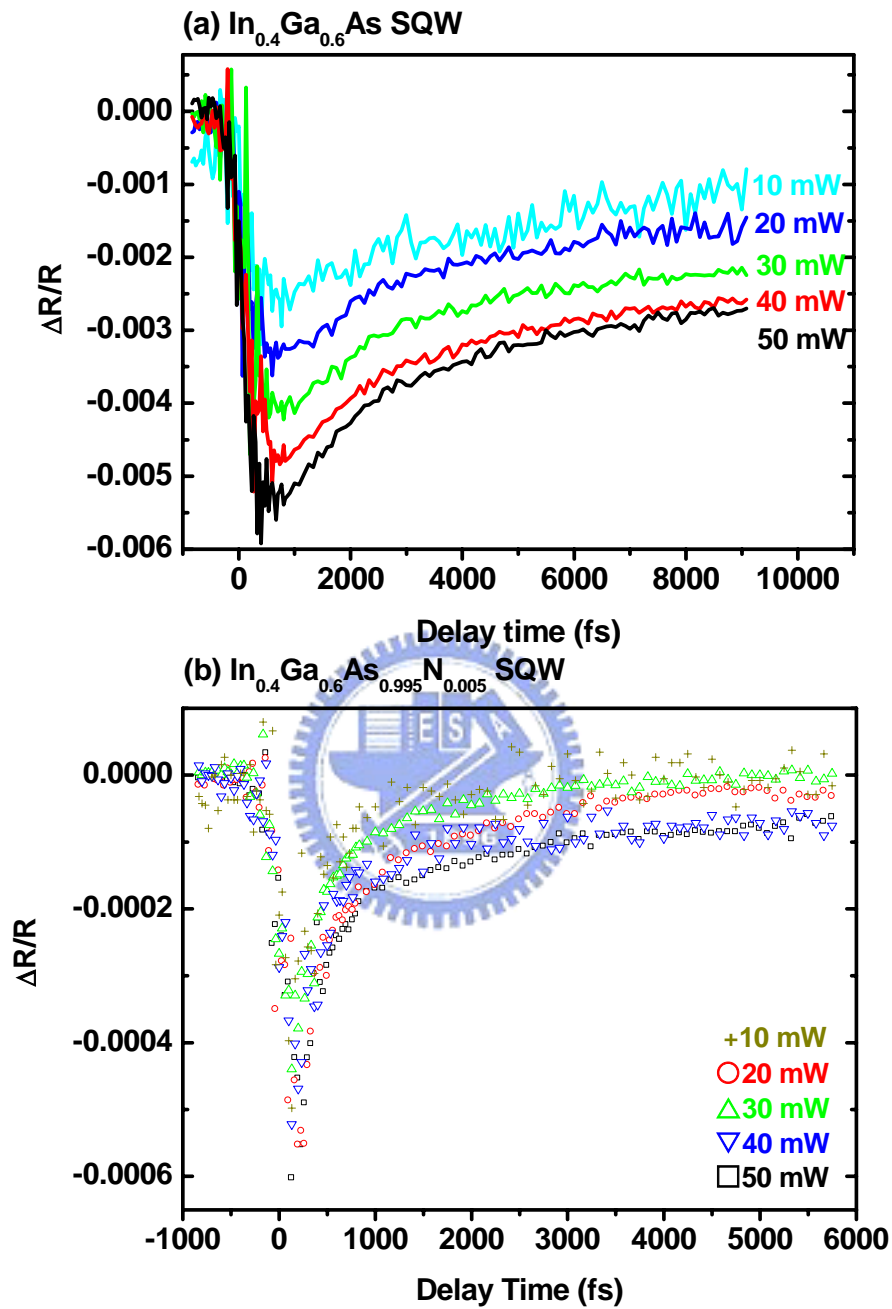


Fig. 5-5 The pump-intensity dependent time-resolved photorefectance of (a) $\text{In}_{0.4}\text{Ga}_{0.6}\text{As}$ SQW. (b) $\text{In}_{0.4}\text{Ga}_{0.6}\text{As}_{0.995}\text{N}_{0.005}$ SQW at 800 nm.

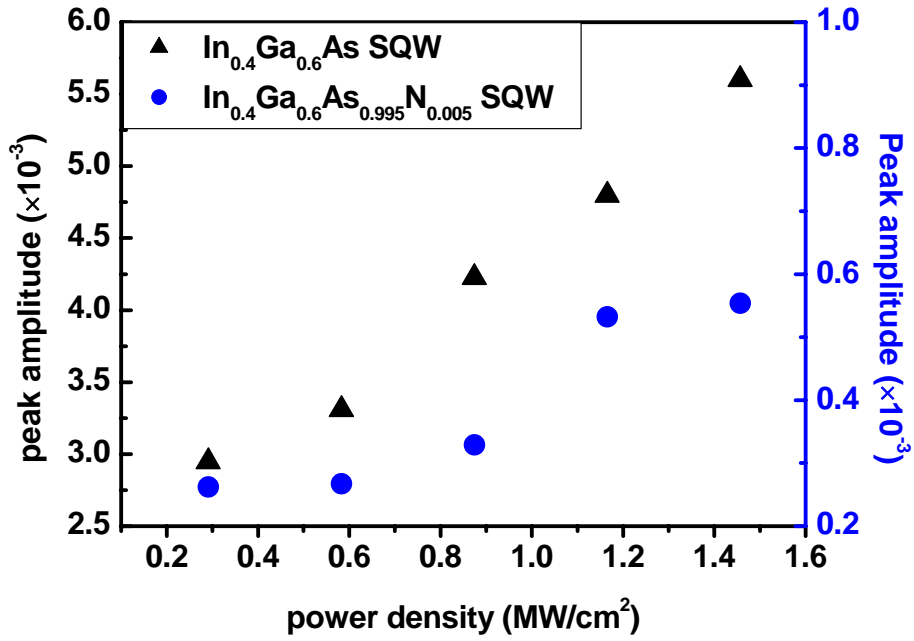


Fig. 5-6 The measured ΔR peak amplitude versus pump power of $\text{In}_{0.4}\text{Ga}_{0.6}\text{As}$ SQW (solid triangle) and $\text{In}_{0.4}\text{Ga}_{0.6}\text{As}_{0.995}\text{N}_{0.005}$ SQW (solid circle).

Table 5-1 List of carrier lifetimes of $\text{In}_{0.4}\text{Ga}_{0.6}\text{As}$ SQW and $\text{In}_{0.4}\text{Ga}_{0.6}\text{As}_{0.995}\text{N}_{0.005}$ SQW with various pump power.

Power density (MW/cm ²)	$\text{In}_{0.4}\text{Ga}_{0.6}\text{As}$		$\text{In}_{0.4}\text{Ga}_{0.6}\text{As}_{0.995}\text{N}_{0.005}$	
	τ_1 (ps)	τ_2 (ps)	τ_1 (ps)	τ_2 (ps)
0.5827	2.92	--	0.311	10.697
0.8741	2.568	--	0.31	10.588
1.1654	2.371	21.586	0.348	6.188
1.4568	1.872	10.562	0.254	1.458

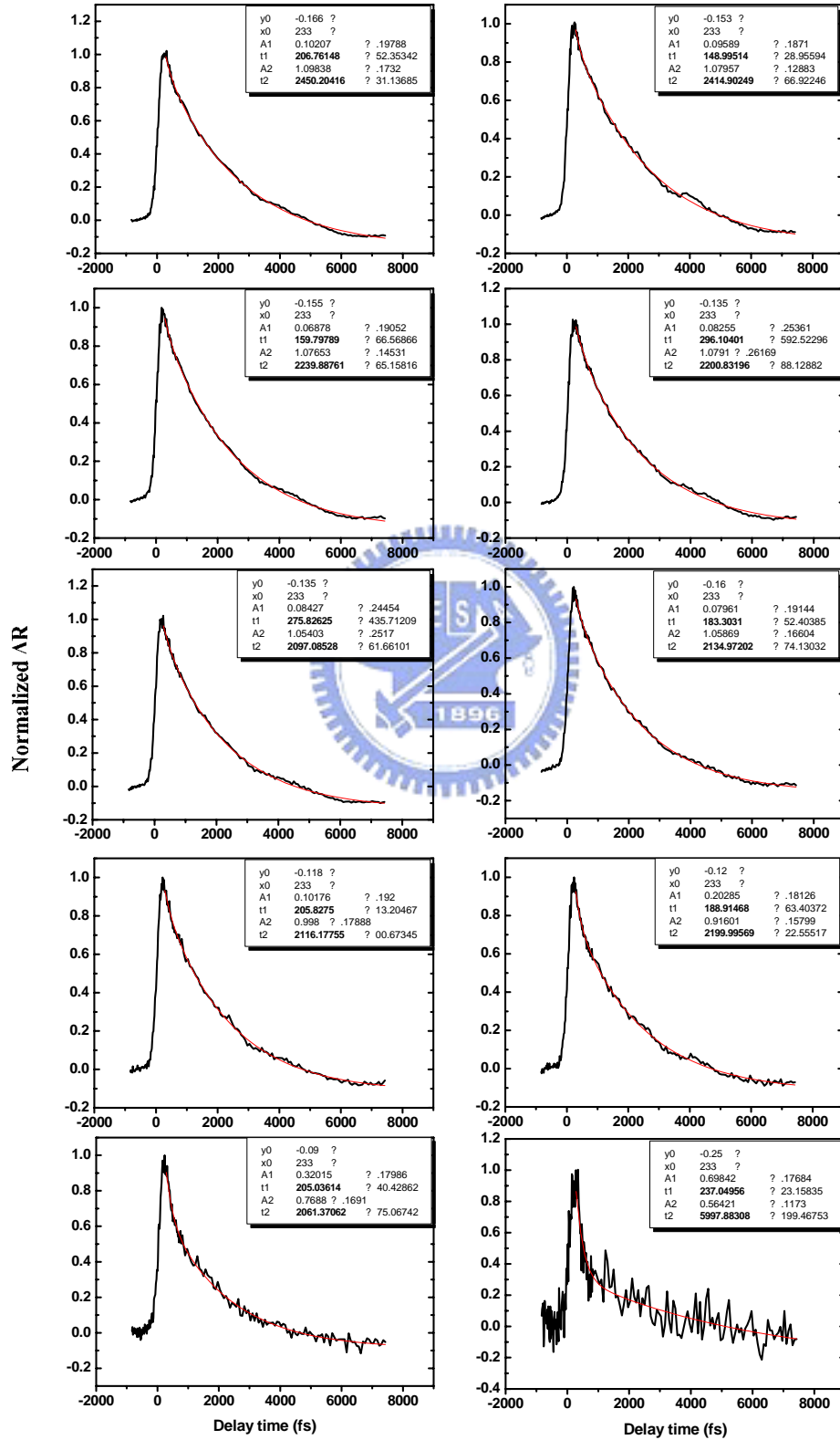
Chapter 6 Conclusion and Perspectives

In this thesis, the ultrafast time-resolved photoreflectance of GaAs and $\text{InGaAs}_x\text{N}_{1-x}$ ($x = 0\%$ and $x = 0.5\%$) single quantum wells are shown. In bulk GaAs, the initially short carrier lifetime from the time-resolved photoreflectance measurements was found not change with increasing the pump power. This confirms that the decaying is due to carrier-phonon scattering. The nonlinear relation between the peak amplitude of ΔR and the pump power is due to carrier-carrier scattering and the induced bandgap shrinkage.

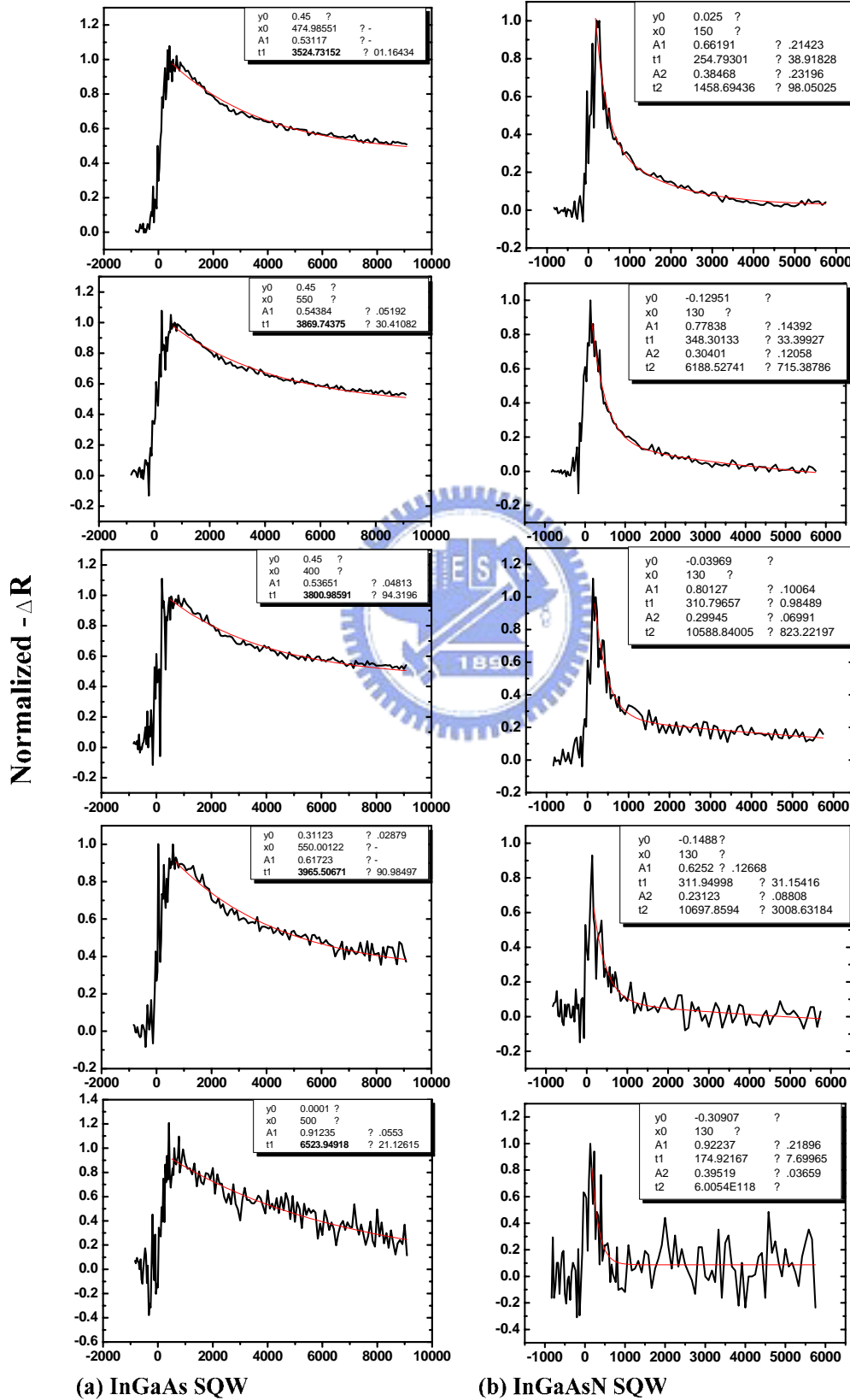
In comparison with the ultrafast time-resolved photoreflectance of $\text{In}_{0.4}\text{Ga}_{0.6}\text{As}$ SQW and $\text{In}_{0.4}\text{Ga}_{0.6}\text{As}_{0.995}\text{N}_{0.005}$ SQW, striking differences are found in the maximum nonlinearity and the carrier relaxation even with such thin single quantum wells of only 6nm within 300 nm wide defining layers. For fixed photon energy, the carrier relaxation for $\text{In}_{0.4}\text{Ga}_{0.6}\text{As}_{0.995}\text{N}_{0.005}$ SQW is faster than for $\text{In}_{0.4}\text{Ga}_{0.6}\text{As}$ SQW. The carrier dynamics is strongly affected by N incorporation. The origin of negative dip is complicated and does not fully understand at the moment, it needs further investigation.

Although we have succeeded in demonstrating the ultrafast time-resolved photoreflectance measurements, there are still many experimental knacks waiting for improvement. First, the pump beam modulation by optical chopper could be replaced by AOM modulator to increase the signal to noise ratio. Second, the pump lens with the shorter focal length may be used to increase the pump density to lift the photoexcitation densities. Third, to tune laser wavelength so that one can make the laser wavelength resonate with the bandgap of the samples.

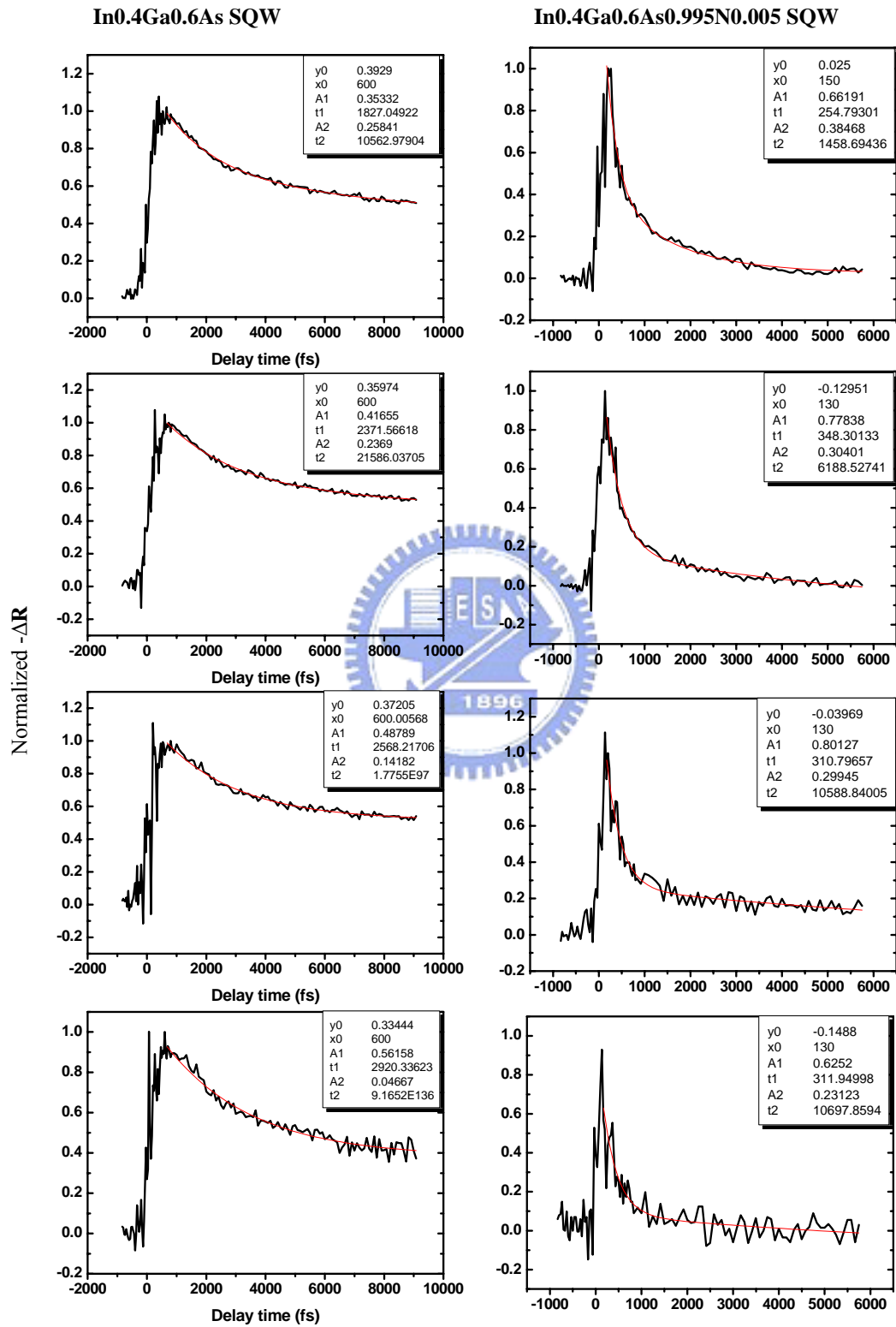
Appendix I Fitting results of bulk GaAs



Appendix II Fitting results of SQW (I)



Appendix III Fitting results of SQW (II)



References

- [1] A. Polimeni, G. Baldassari Hoyer von Hogersthal, M. Bissiri, M. Capizzi, A. Frova, M. Reinhardt, and A. Forchel, *Semicond. Sci. Technol.*, **17**, 797 (2002).
- [2] C. Ellmers, F. Hohnsdorf, J. Koch, C. Agert, S. Leu, D. Karaiskaj, M. Hofmann, W. Stolz, and W. W. Ruhle, *Appl. Phys. Lett.*, **74**, 2271 (1999).
- [3] N. Tansu, J. Y. Yeh, and L. Mawst, *IEEE J. Sel. Topics Quantum Electron.*, **9**, 1220 (2003).
- [4] J. Y. Yeh, N. Tansu, and L. J. Mawst, *Electron Lett.*, **40**, 739 (2004).
- [5] H. P. Xin, and C. W. Tu, *Appl. Phys. Lett.*, **72**, 2442 (1998).
- [6] G. L. Belenky, C. L. Reynolds, D. V. Donetsky, G. E. Shtengel, M. S. Hybertsen, M. A. Alam, G. A. Baraff, R. K. Smith, R. F. Kazarinov, J. Winn, and L. E. Smith, *IEEE J. Quantum Electron.*, **35**, 1515 (1999).
- [7] O. Anton, C. S. Menoni, J. Y. Yeh, L. J. Mawst, J. M. Pikal, and N. Tansu, *IEEE Photon. Technol. Lett.*, **17**, 953 (2005).
- [8] R. A. Mair, J. Y. Lin, H. X. Jiang, E. D. Jones, A. A. Allerman, and S. R. Kurtz, *Appl. Phys. Lett.* **76**, 188 (2000).
- [9] I. A. Buyanova, G. Pozina, P. N. Hai, N. Q. Thinh, J. P. Bergman, W. M. Chen, H. P. Xin and C. W. Tu, *Appl. Phys. Lett.*, **77**, 2325 (2000).
- [10] A. Kaschner, T. Lu ttgert, H. Born, A. Hoffmann, A. Yu. Egorov and H. Riechert, *Appl. Phys. Lett.*, **78**, 1391 (2001).
- [11] A. Vinattieri, D. Alderighi, M. Zamfirescu, M. Colocci, A. Polimeni, M. Capizzi, D. Gollub, M. Fischer, and A. Forchel, *Appl. Phys. Lett.*, **82**, 2805 (2003).
- [12] Andreas Othonos, *J. Appl. Phys.*, **83**, 1789 (1998).
- [13] R. L. Fork, B. I. Greene, and C. V. Shank, *Appl. Phys. Lett.*, **38**, 671 (1981).
- [14] D. J. Bradely *et al.*, *Appl. Phys. Lett.*, **16**, 53 (1970).
- [15] M. Schelev *et al.*, *Appl. Phys. Lett.*, **18**, 354 (1971).
- [16] B. L. Liu, B. Liu, and Z. Y. Xu, *J. Appl. Phys.*, **90**, 5111 (2001).
- [17] A. Leitenstorfer, C. Furst, A. Laubereau, W. Kaiser. *Phys. Rev. Lett.*, **26**, 1545 (1996).
- [18] M. Schall, P. U. Jepsen, *Opt. Lett.*, **25**, 13 (2000).
- [19] M. C. Beard, G. M. Turner, C. A. Schmuttenmaer, *Phys. Rev. B.*, **15**, 15764 (2000).
- [20] F. Kadlec, H. Nemeč, and P. Kuzel, *Phys. Rev. B.*, **70**, 125205 (2004).
- [21] J. Shah, *Ultrafast Spectroscopy of Semiconductors and Semiconductor Nanostructures*, Springer-Verlag, Berlin, (1996).
- [22] D. H. Auston, S. McAfee, C. V. Shank, E. P. Ippen, and O. Teschke, *Solid-State*

- Electron.*, **21**, 147 (1978).
- [23] C. V. Shank, R. L. Fork, R. F. Leheny, and J. Shah, *Phys. Rev. Lett.*, **42**, 112 (1979).
- [24] R. W. Schoenlein, W. Z. Lin, S. D. Brorson, E. P. Ippen, and J. G. Fujimoto, *Solid-State Electron.*, **31**, 443 (1988).
- [25] X. Q. Zhou, K. Leo, and H. Kurz, *Phys. Rev. B.*, **45**, 3886 (1992).
- [26] G. Sucha, S. R. Bolton, D. S. Chemla, D. L. Sivco, and A. Y. Cho, *Appl. Phys. Lett.*, **65**, 1486 (1994).
- [27] P. Borri, W. Langbein, J. M. Hvam, and F. Martelli, *Phys. Rev. B.*, **59**, 2215 (1999).
- [28] P. Bhattacharya, S. Ghosh, S. Pradhan, J. Singh, W. Zong-Kwei, J. Urayama, K. Kim, and T. B. Norris, *IEEE J. Quantum Electronics.*, **39**, 952 (2003).
- [29] L. Grenouillet, C. Bru-Chevallier, G. Guillot, P. Gilet, P. Duvaut, C. Vannuffel, A. Million, and A. Chenevas-Paule, *Appl. Phys. Lett.*, **76**, 2241 (2000).
- [30] N. Tansu, N. J. Kirsch, and L. J. Mawst, *Appl. Phys. Lett.*, **81**, 2523 (2002).
- [31] N. Tansu, J. Y. Yeh, and L. J. Maest, *Appl. Phys. Lett.*, **82**, 3008 (2003).
- [32] N. Tansu, J. Y. Yeh, and L. J. Maest, *Appl. Phys. Lett.*, **82**, 4038 (2003).
- [33] H. C. Kuo, F. I. Lai, Y. H. Chang, M. Y. Tsai, S. Y. Kuo, S. C. Wang, N. Tansu, J. Y. Yeh, and L. J. Maest, *J. J. Appl. Phys.*, in press.
- [34] Lifang Xu, D. Patel, G. Vaschenko, O. Anton, C. S. Menoni, J. Y. Yeh, T. T. V. Roy, L. J. Mawst, N. Tansu, CLEO/QELS '05, Baltimore, Maryland, USA.
- [35] W. Z. Lin, R. W. Schoenlein, J. G. Fujimoto, and E. P. Ippen, *IEEE J. Quantum Electronics.*, **24**, 267 (1988).
- [36] W. Z. Lin, R. W. Schoenlein, E. P. Ippen and R. A. Logan, *Appl. Phys. Lett.*, **50**, 124 (1987).
- [37] S. U. Dankowski, D. Streb, M. Ruff, P. Kiesel, M. Kneissl, B. Knuepfer, G. H. Doehler, U. D. Keil, C. B. Sorenson, and A. K. Verma, *Appl. Phys. Lett.*, **68**, 37 (1996).
- [38] J. A. Kash, J. C. Tsang, and J. M. Hvam, *Phys. Rev. Lett.*, **54**, 2151 (1985).
- [39] P. A. Wolff, *Phys. Rev.*, **126**, 405 (1962).
- [40] M. Levinshtein, S. Romyantsev, M. Shur, *Handbook series on semiconductor parameters*, World Scientific, (1996)
- [41] W. Z. Lin, J. G. Fujimoto, E. P. Ippen, R. A. Logan, *Appl. Phys. Lett.*, **51**, 161 (1987).
- [42] J. Micallef *et al.*, *Appl. Phys. Lett.*, **62**, 3164 (1993).
- [43] B. R. Bennett, R. A. Soref, and J. A. D. Alamo, *IEEE J. Quantum Electronics.*, **26**, 113 (1990).
- [44] S. sinning, T. Dekorsy, and M. Helm, *IEE Proc.-Optoelectron.*, **151**, 361 (2004)..